

# The demise of the Last Interglacial recorded in isotopically dated speleothems from the Alps

Michael C. Meyer<sup>a,\*</sup>, Christoph Spötl<sup>a</sup>, Augusto Mangini<sup>b</sup>

<sup>a</sup>*Institut für Geologie und Paläontologie, Universität Innsbruck, Innsbruck, Austria*

<sup>b</sup>*Forschungsstelle Radiometrie, Heidelberger Akademie der Wissenschaften, Heidelberg, Germany*

Received 27 June 2007; received in revised form 9 November 2007; accepted 13 November 2007

## Abstract

The transition from interglacial to glacial climate has attracted much attention in paleoclimatic research, partly because orbital forcing dictates that such a return to a new ice age is inescapable (albeit in the distant future only). The detailed series of steps that leads to glacial inceptions remains poorly understood, however, and studies of past glacial inceptions are often compromised by incomplete records, imprecise chronological control, and/or uncertainties associated with proxy-transfer functions. Here we present results from U–Th-dated speleothems from a cave in the Austrian Alps (Entrische Kirche cave) which grew continuously between ca 127 and 114 ka and intermittently also during subsequent stadials and interstadials. The alpine setting of this cave is prone to periglacial and glacial processes as well as temperature and precipitation changes which are recorded in these cave deposits. We use high-resolution stable isotope data to constrain paleoenvironmental changes associated with the demise of the Last Interglacial, unprecedented in detail for central Europe. Peak interglacial conditions are characterized by high  $\delta^{18}\text{O}$  values and high growth rates from ca 127 to 124 ka. A major drop in  $\delta^{18}\text{O}$  by 3‰ occurred at ca 118 ka, which coincided with cold event C26 in the North Atlantic. This isotopic shift, which occurred at or close to isotopic equilibrium, cannot be explained by simple uniform cooling. Modelling suggests that enhanced seasonality, dominated by significant changes in winter precipitation, are required to reconcile the isotope data with the fact that calcite deposition continued across the MIS 5e/d transition (i.e., no cave freezing). This period of enhanced seasonality lasted for several millennia during which the catchment area of the cave remained geomorphologically stable and ice free. Eventually, speleothem growth terminated at ca 114 ka, which is in line with widespread ice-rafting in the North Atlantic (cold event C24) and the onset of fully stadial conditions during MIS 5d. © 2007 Elsevier Ltd. All rights reserved.

## 1. Introduction

Interglacial periods represent only a small fraction of the Quaternary when sea level reached a maximum, the extent of continental and mountain glaciation was minimal and temperatures were broadly similar to today. The Last Interglacial, although not a perfect analogue for the Holocene because of different orbital parameters (Loutre and Berger, 2003), has received most attention and detailed records e.g. of the terrestrial vegetation (e.g., Sánchez Goñi et al., 1999; Drescher-Schneider, 2000; Tzedakis, 2003; Klotz et al., 2004; Brauer et al., 2007; Müller and Sánchez Goñi, 2007) and the temperature distribution of the ocean's

surface waters at that time exist (Lehman et al., 2002; Rasmussen et al., 2003; Martrat et al., 2004; Oppo et al., 2006). Despite these and many other studies significant uncertainties remain and most of these boil down to imprecise chronologies and poorly understood climate-proxy-transfer functions.

Recent years have seen increasing awareness of speleothems as precise recorders of past climate change. The strength of these abiogenic carbonate deposits lies both in their superior chronology based on U-series dating (Henderson, 2006) and the fact that their main proxy, the oxygen isotopic composition, is the same as in ice. Alpine speleothems (as well as speleothem records from several other settings in the Northern Hemisphere) can thus be more directly compared to the high-latitude ice cores than e.g. paleovegetation data from lake sediments, because the  $\delta^{18}\text{O}$  values of these cave calcites and of the Greenland ice

\*Corresponding author. Current address: School of Earth and Environmental Sciences, University of Wollongong, NSW, Australia.  
E-mail address: meyer@uow.edu.au (M.C. Meyer).

cores shift in the same direction in response to paleoclimatic change (e.g., Wurth et al., 2004; McDermott et al., 2005; Spötl et al., 2006). One of the key sites for speleothem records spanning the Last Interglacial in Europe is the high-alpine Spannagel Cave in the Central Alps of Austria. Stalagmite and flowstone samples recorded the onset of warm conditions 129–130 ka ago (Spötl et al., 2007), now regarded as the first well-dated evidence of interglacial conditions in central Europe (Sirocko et al., 2007). While this date is consistent with other U–Th-dated speleothem records from Italy (Drysdale et al., 2005) and Israel (Bar-Matthews et al., 2003), it is in slight conflict with indirectly dated evidence for the beginning of the Last Interglacial from marine (Shackleton et al., 2003) and lacustrine sequences (Brauer et al., 2007). The end of the Last Interglacial is recorded in Spannagel Cave samples by a hiatus at 118–119 ka (Spötl et al., 2007). Given the present-day low temperature of Spannagel Cave this high-alpine system reacts sensitively to cooling events (i.e. termination of speleothem growth) and none of the Last Interglacial speleothems from this site grew beyond 118 ka, whereas U–Th-dated corals indicate an interglacial sea-level highstand until  $116 \pm 1$  ka (Stirling et al., 1998). Speleothems in caves located at lower elevation and hence higher temperature in the Alps, however, provide the opportunity to potentially preserve a more complete history of the

glacial inception. Here we present data from a flowstone found in Entrische Kirche, an inneralpine cave some 110 km east of Spannagel Cave, which, to our knowledge, is the first directly dated, continuous stable isotope record of the demise of the Last Interglacial at least within central Europe.

## 2. Setting of the cave

Entrische Kirche is situated in the central part of the Eastern Alps, ca 25 km north of the main alpine crest, where the highest summits of the Eastern Alps are located (Großglockner 3798 m, Fig. 1). The distance from the cave to the northern fringe of the Alps is ca 55 km. The cave opens at 1040 m on the steep, eastern flank of the Gastein Valley which forms a gorge prior to entering the main Salzach Valley. The area east of the cave reaches up to 2119 m in elevation. Alpine mats and shrubs constitute the vegetation cover above the timberline (ca 1800–1900 m). Two small lakes are present at 1856 and 1949 m, respectively, surrounded by steep slopes.

The cave is cut in Jurassic calcite mylonites (Klammkalk) which absorbed a considerable amount of largely ductile deformation in response to oblique plate convergence during the Tertiary orogeny (Exner, 1979; Peer and Zimmer, 1980). The host rock is characterized by an E-W

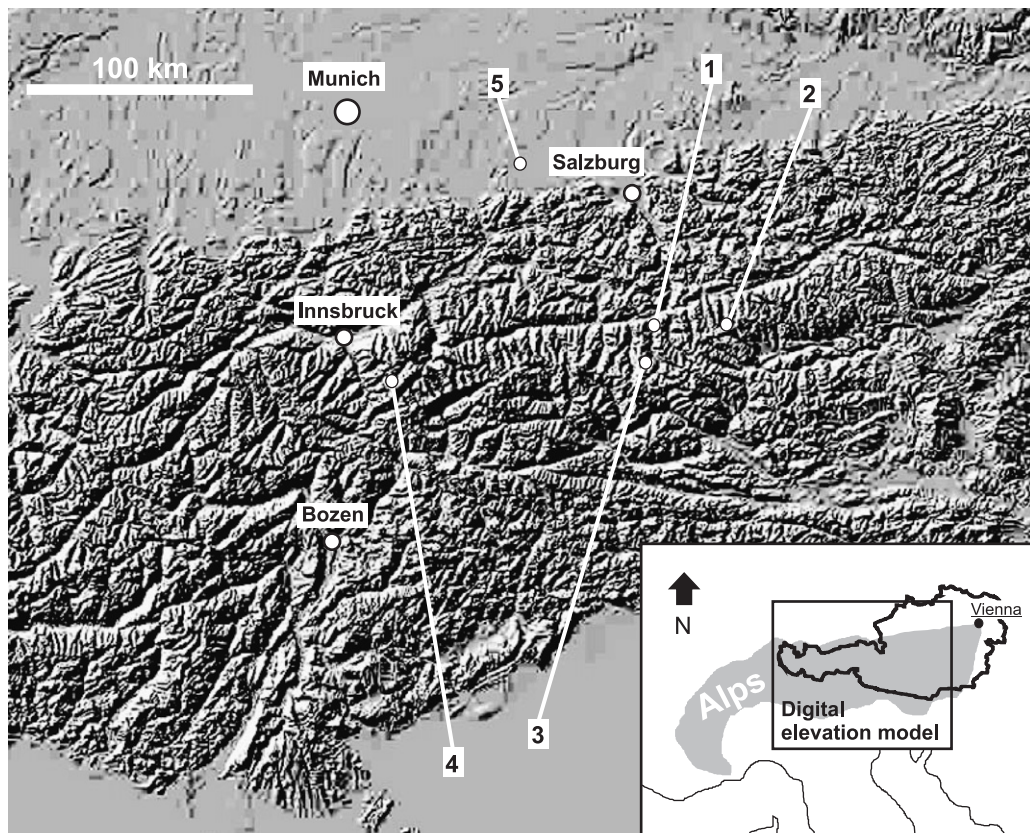


Fig. 1. Digital elevation map of the central part of the Austrian Alps showing location of Entrische Kirche cave (1), as well as of other relevant sites mentioned in the text: Obertauern (2), Böckstein (3), Spannagel Cave (4), Samerberg (5).

trending stretching lineation, upright folds with E-W oriented axes and sinistral strike-slip faults, which are generally ENE trending and dipping steeply towards N (Wang and Neubauer, 1998). At the largest scale folding is responsible for the morphology in the local catchment area, where e.g. anticlines form the backbone of mountain ridges and synclines host high-alpine lakes. The cave passages are bound to these E-W oriented tectonic structures and are arranged in two levels. The lower level extends—gently increasing in elevation—270 m in W-E direction, and is connected via shafts to the upper level, ca 55 m higher up. The total surveyed length of the cave is 1.6 km (Klappacher, 1992). Passages with elliptical cross sections alternate with cave halls which are partly collapsed. A perennial stream with a peak discharge of ca 10 l/s drains the lower cave level. Cave waters infiltrate in a small catchment (ca 3 km<sup>2</sup>) at an elevation of ca 1800–2100 m. Tracer experiments demonstrated a direct connection between a ponor on the shore of one of the lakes on top of the mountain and the cave stream in the lower level of the Entrische Kirche (transit time 1–3 days, horizontal distance: 1.8 km; Ganahl, 1991).

The interior cave air temperature is 5.5 °C which is identical to the mean annual air temperature (MAAT) outside the cave. Mean annual precipitation (MAP) at 1100 m is ca 1100 mm and ca 1500 mm in the catchment area on top of the mountain (data based on a regional network of meteorological stations in the southern part of the province of Salzburg—[www.zamg.ac.at/fix/klima/oe71-00](http://www.zamg.ac.at/fix/klima/oe71-00)). The dominant wind direction responsible for moisture transport to the study area is from the northwest (Steinhauser, 1982; Lauscher, 1985; ZAMG, 1985).

The catchment area is unglaciated and was so during the entire Holocene. During glacial maxima such as Marine Isotope Stage (MIS) two ice streams flowing north from the main alpine crest reached an elevation of ca 2000–2100 m in the study area (van Husen, 1987) burying almost the entire catchment of Entrische Kirche under ice.

The cave hosts both active and fossil flowstones, stalagmites, stalactites and soda straws, as well as clastic sediments (loam, silt, sand and gravel). This study focuses on flowstone samples obtained from the upper level of the cave. A large flowstone is present at the base of the Teufelskrallen shaft (termed TKS). This conical formation is ca 4 m in height and shows a basal diameter of ca 1.8 m (Fig. 2). The flowstone is currently inactive and covered by medium-grey calcite (as opposed to active, white calcitic stalagmites also present on this cave level) and was probably originally fed by fissure flow. We focus here on the topmost 30 cm of four parallel drill cores, TKS I, II, III, and IV, retrieved from the lower part of the flowstone formation (Fig. 2). A fragment of a second, much smaller and inactive flowstone (ENT 10) was found detached from its substrate in a small chamber a few tens of metres below the TKS site. This flowstone layer is ca 8 cm thick and was studied for comparison purpose.



Fig. 2. The TKS flowstone and location of drill cores.

### 3. Methods

Core samples were examined both macroscopically and in thin-sections using transmitted-light and epifluorescence microscopy. Subsamples for stable carbon and oxygen isotope analyses were obtained at 0.2 mm increments with a Merchantek micromill and analysed using a ThermoFinnigan Delta<sup>Plus</sup>XL mass spectrometer. The analytical precision (1 sigma) is typically 0.08‰ for  $\delta^{18}\text{O}$  and 0.06‰ for  $\delta^{13}\text{C}$  (Spötl and Vennemann, 2003). For U–Th age determination 20 subsamples were retrieved along the TKS I, II and IV drill cores. Two subsamples were analysed from the ENT 10 hand specimen (see Table 1). Subsamples were either cut using a diamond band saw or milled using a hand-held dental drill. The thickness of the individual subsamples for U–Th dating ranges from 2 to 10 mm. Chemical preparation followed a standard protocol (Scholz et al., 2004) and U–Th measurements were performed on a thermal ionisation mass spectrometer (Finnigan MAT 262 RPQ) with a double filament technique. The calibration of the U and Th spikes used in the Heidelberg Laboratory is described in Hoffmann et al. (2007). All ages were calculated using the half lives reported by Cheng et al. (2000). All ages were corrected for detrital contamination assuming a  $^{232}\text{Th}/^{238}\text{U}$  mass ratio of 3.8.

Table 1

U–Th ages of the TKS cores and the ENT 10 flowstone (DFT = distance from top, corr. = corrected, abs. = absolute, uncorr. = uncorrected)

Laboratory no.	Sample	DFT (mm)	$\delta U$ (corr.) (%)	Error (abs.)	$^{238}U$ ( $\mu g/g$ )	Error (abs.)	$^{232}Th$ (ng/g)	Error (abs.)	$^{230}Th$ (pg/g)	Error (abs.)	Age uncorr. (ka)	Age corr. (ka)	Error (ka)
4085	TKS II (7.1)	107.0	89.1	5.2	0.15193	0.00030	2.591	0.014	1.800	0.016	116.8	116.4	2.2
3715	TKS I (11.0)	107.6	82.1	4.3	0.1570	0.0003	1.1552	0.0103	1.81	0.03	113.2	113.0	3.5
3862	TKS I (11.5)	114.6	76.3	6.3	0.1432	0.0003	6.2096	0.0416	1.66	0.03	115.7	114.6	3.5
4086	TKS II (8.2)	118.0	90.2	7.2	0.13094	0.00026	3.473	0.030	1.558	0.036	117.4	116.8	5.0
3871	TKS I (13.2)	131.0	91.2	3.9	0.13545	0.00027	2.237	0.010	1.599	0.016	115.6	115.1	2.2
4087	TKS II (9.7)	133.0	79.9	5.1	0.16059	0.00032	1.711	0.010	1.875	0.026	115.7	115.4	3.0
4088	TKS II (10.4)	140.0	77.4	6.6	0.13173	0.00026	0.7645	0.0050	1.552	0.019	118.1	117.9	2.9
4089	TKS II (11.0)	146.0	90.0	3.7	0.14194	0.00028	1.586	0.005	1.708	0.015	119.8	119.5	2.0
3872	TKS I (15.1)	148.0	69.6	5.7	0.19731	0.00039	1.988	0.026	2.308	0.035	118.4	118.1	3.4
4090	TKS II (11.5)	151.0	81.9	5.2	0.11943	0.00024	1.3630	0.0080	1.440	0.024	122.0	121.8	3.9
4092	TKS II (14.3)	179.0	75.2	5.2	0.22808	0.00046	0.8068	0.0045	2.717	0.019	121.0	120.9	2.0
3818	TKS IV (19.0)	190.0	86.2	3.1	0.23804	0.00048	1.185	0.011	2.917	0.050	124.7	124.6	4.0
4148	TKS II (15.7)	193.0	74.2	4.8	0.30544	0.00061	0.8813	0.0048	3.634	0.029	120.9	120.9	2.1
4200	TKS II (16.3)	199.0	76.5	2.7	0.32798	0.00066	1.1476	0.0029	3.969	0.015	124.2	124.1	1.2
4201	TKS II (17.3)	209.0	71.8	3.3	0.32973	0.00066	0.9922	0.0085	3.995	0.028	125.6	125.5	1.8
4149	TKS II (18.5)	221.0	74.2	2.9	0.27686	0.00055	1.3332	0.0028	3.374	0.010	126.4	126.2	1.1
3711	TKS I (30.0)	295.6	69.7	3.7	0.28893	0.00058	1.704	0.013	3.506	0.042	126.5	126.4	3.0
4150	TKS II (25.4)	300.0	68.0	3.9	0.26023	0.00052	3.650	0.014	3.166	0.017	127.5	127.2	1.7
3709	TKS I (34.5)	336.0	59.2	1.6	1.0823	0.0011	91.013	0.491	13.068	0.041	128.34	126.09	0.86
3708	TKS I (37.4)	369.6	54.5	3.5	0.6570	0.0013	15.094	0.080	7.824	0.086	126.0	125.4	2.7
R146	ENT 10A	20.0	81.1	1.4	0.0965	0.0003	1.2521	0.0085	1.1432	0.0132	118.46	118.16	2.52
R147	ENT 10B	68.0	70.4	1.4	0.1344	0.0004	0.8448	0.0058	1.5979	0.0135	121.67	121.44	1.92

Twenty subsamples taken from cores TKS I, II and IV were referenced to the stratigraphy of core TKS I and cover the white calcite sequence (107–369.6 mm). Errors are quoted as  $2\sigma$  standard deviations. Ages were corrected for initial detrital  $^{230}Th$  under the assumption of an activity ratio of  $^{230}Th/^{232}Th$  analogous to the average crust.

## 4. Flowstone properties

### 4.1. Petrography

All four TKS drill cores reveal the same distinctive succession of calcite units, although the thickness of individual units differs slightly between the cores. We use core TKS II to illustrate the macroscopic stratigraphy of the TKS flowstone (Fig. 3). The basal ca 200 mm (from 70 to 260 mm) are composed of white, translucent, inclusion-poor calcite. In all cores this calcite unit is dense and non-laminated below ca 110 mm and becomes progressively more laminated above with lamina thicknesses on the sub-mm scale (Fig. 3). At 70 mm the white calcite is abruptly overlain by variably brown, detrital-rich calcite, where layers of 5–15 mm thick calcite showing a dendritic macrofabric alternate with mm- to cm-thin laminated calcite. A 4 mm thick white laminated calcite layer is sandwiched in the brownish laminated calcite sequence at 68 mm of the cores TKS I and IV but is less well developed in core TKS II.

The sharp macroscopic transition from the white, laminated calcite to the brownish detrital-rich calcite (at 70 mm) strongly suggests a growth interruption (hiatus H1, Fig. 3). At 32 mm growth of brown laminated calcite apparently ceased again and was overlain sharply by dendritic calcite. This abrupt transition—a preferential fracture plane in all drill cores—is regarded as a second hiatus (H2, Fig. 3).

This study focuses on the white calcite sequence for which the microscopic characteristics are described in detail in the supplementary online material (SOM) 1 and are only briefly summarized here. The white calcite is composed of a columnar fabric and reveals faint fluorescent microbanding (3–100  $\mu m$  laminae) which, however, is not present throughout this sequence. The hiatus H1, separating the white, translucent from the brown detrital calcite sequence, reveals clear-cut corrosion features on the microscopic scale (SOM 1).

The ENT 10 sample is composed of white calcite, which shows a hiatus at 20 mm (H1) with brown laminated calcite overlying white translucent calcite. From 20 to 40 mm the white translucent calcite is dense and macroscopically laminated. These sub-mm laminae can be traced throughout the entire specimen.

### 4.2. Stable oxygen isotopes

Continuous, high-resolution stable isotope profiles were obtained for the TKS cores I, II and IV, as well as for the ENT 10 hand-specimen and show the same trends (Fig. 4). Calcite growth started with  $\delta^{18}O$  values of ca  $-10.4\%$  followed by a trend towards higher values up-section (up to  $-8\%$ , mean  $-8.7\%$ ). Regular high-frequency cycles are superimposed on this trend with amplitudes of 1–2%. Within ca 2 cm the O isotope values then decrease steeply by 4% (from  $-8\%$  to  $-12\%$  using the maximum and

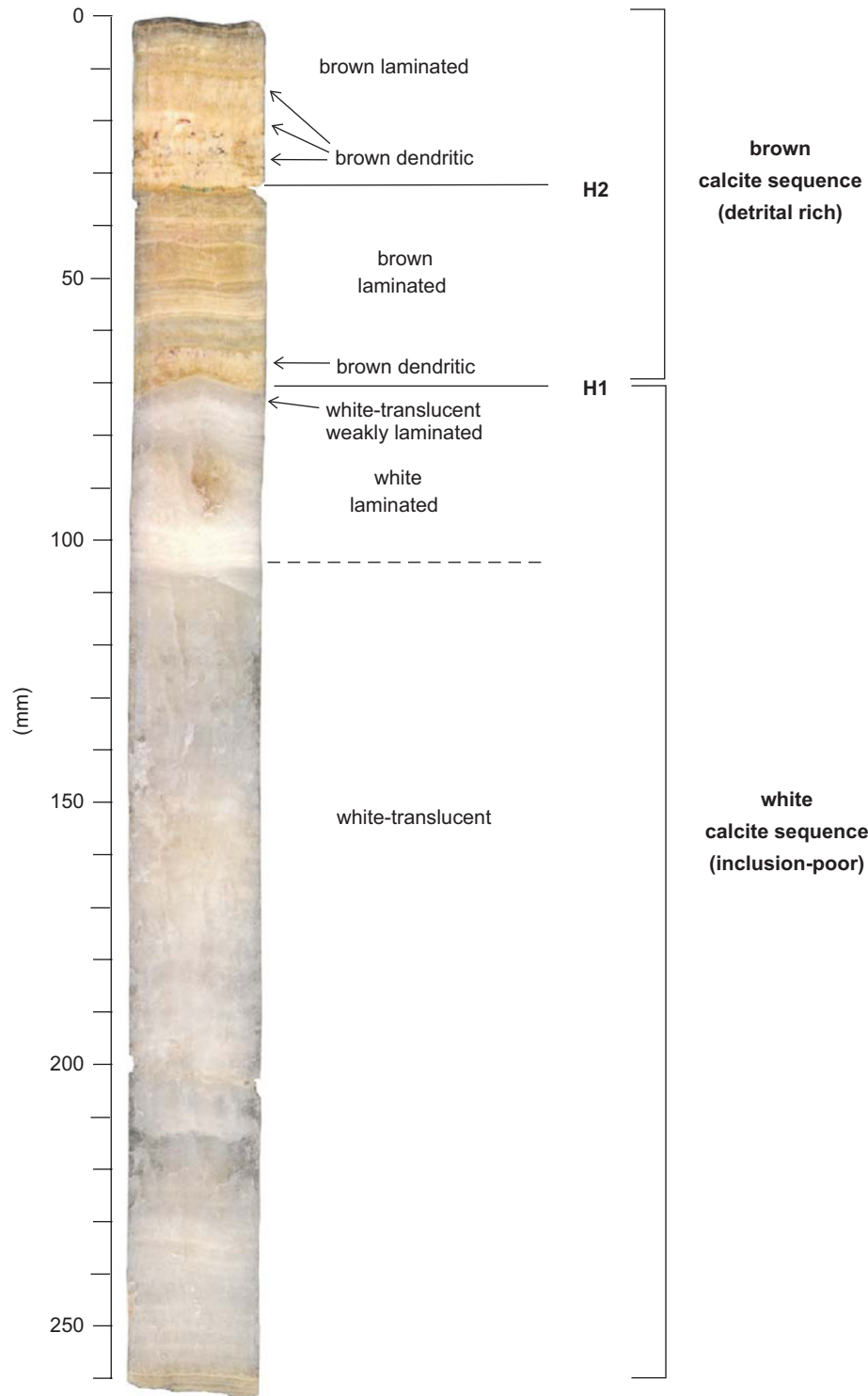


Fig. 3. Macroscopic petrography of core TKS II representative of the stratigraphy of the TKS flowstone. H1 and H2 are hiati.

minimum values, respectively) and remain at a much lower level throughout the rest of the core (mostly  $-12\text{‰}$  to  $-10\text{‰}$ ). This sudden isotopic shift was reproduced in all three TKS cores as well as in specimen ENT 10. Further up-section, two abrupt jumps towards higher  $\delta^{18}\text{O}$  values were identified at 60 and 104 mm in core TKS I and are

present in the other TKS cores as well. There is a remarkable correspondence between oxygen isotopes and petrography in all TKS cores (Fig. 4), i.e. the trend towards higher  $\delta^{18}\text{O}$  values from 350 to 145 mm and the subsequent 4‰ drop occur within the white, translucent, inclusion-poor calcite sequence, followed by the white, laminated

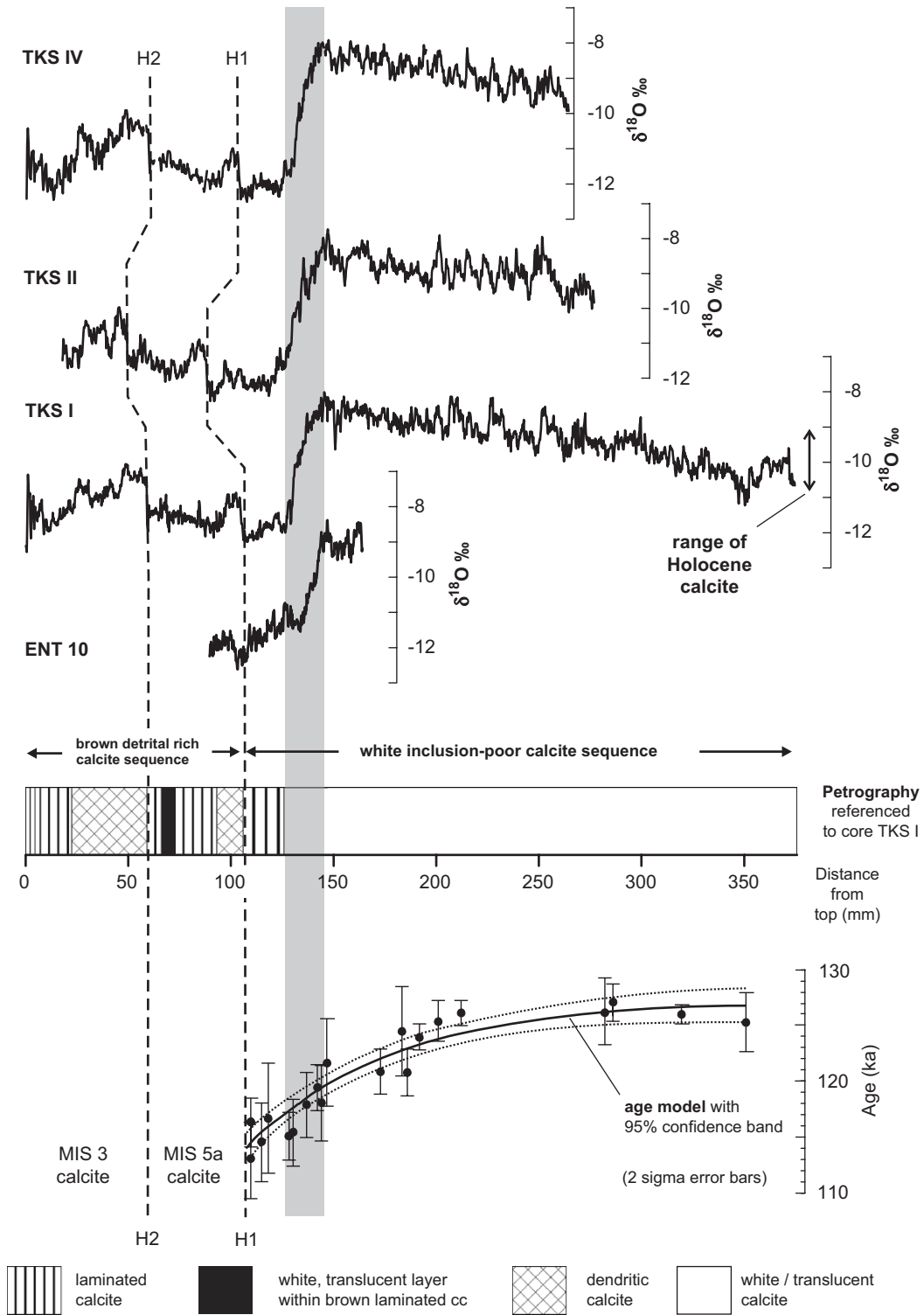


Fig. 4. Oxygen isotope records and stacked age model of the TKS and ENT 10 flowstones. *Top to the left*. All three TKS cores reveal the same isotopic features which can be correlated to the petrography (H1 and H2 are major hiati). The petrographic units are the same as in Fig. 3. Core TKS III (not shown) was not sampled for stable isotopes but shows the same petrographic units. Twenty subsamples from the white translucent and inclusion-poor calcite sequences were used to construct the age model (some data points overlap). The  $\delta^{18}\text{O}$  curve of the ENT 10 flowstone was aligned to the petrography and isotope record of the TKS cores. The vertical grey bar highlights the pronounced 4‰ drop in  $\delta^{18}\text{O}$ . MIS 5e calcite precipitated prior and MIS 5d calcite (see Fig. 6 and text) subsequently to this drop (until hiatus H1).

calcite which reveals consistently low  $\delta^{18}\text{O}$  values of  $-12\%$  to  $-11.5\%$ . The abrupt isotope jumps at 104 and 60 mm correspond to hiatus H1 and H2, respectively. In the

remaining succession the dendritic calcite shows slightly higher  $\delta^{18}\text{O}$  values than the brown laminated calcite (Fig. 4).

A broadly similar stable oxygen isotope record was obtained from sample ENT 10 (Fig. 4). A steep drop in  $\delta^{18}\text{O}$  (starting from  $-8.6\text{‰}$ ) within the white translucent calcite is followed by ca 3 cm of white laminated calcite throughout which isotope values are further decreasing until a minimum value of  $-12.6\text{‰}$  is reached just below hiatus H1. The amplitude of the isotopic drop thus amounts to  $3.8\text{‰}$  with the most rapid descent ( $3\text{‰}$ ) occurring within the white translucent calcite sequence.

### 4.3. Stable carbon isotopes

The  $\delta^{13}\text{C}$  record of all flowstone samples is characterized by a high-amplitude, high-frequency signal with no obvious long-term trends. Within the white calcite succession  $\delta^{13}\text{C}$  minima are between  $-7\text{‰}$  and  $-6\text{‰}$  and positive excursions typically reach  $4\text{‰}$ . In the brown calcite succession amplitudes are similar ( $6\text{‰}$ ) but  $\delta^{13}\text{C}$  minima reach as low as  $-8\text{‰}$  (between H1 and H2, Fig. 5).

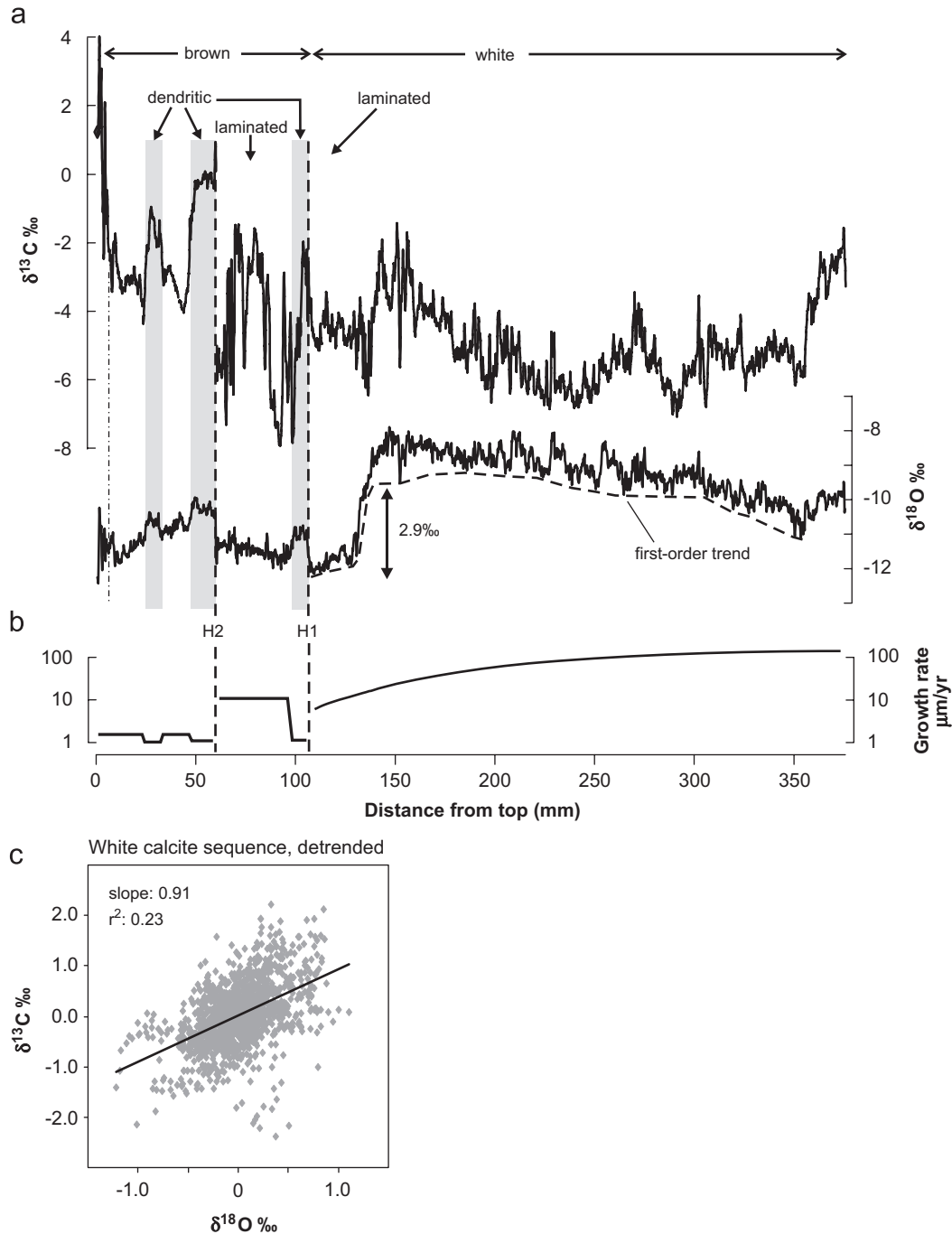


Fig. 5. (a) Stable oxygen and carbon isotope data of the TKS I core. The first-order trend in the  $\delta^{18}\text{O}$  record of the white calcite sequence is drawn along the  $\delta^{18}\text{O}$  minima (dashed line). (b) Flowstone growth rates were calculated from the age model of the white calcite sequence and estimated from the thicknesses of fluorescent laminae in the brown calcite succession, respectively. (c) Cross correlations between carbon and oxygen isotopes. Note that the long-term trend in the data from the white calcite was removed (dashed line in a).

#### 4.4. U–Th chronology

Cores TKS I, II and IV were subsampled for U–Th dating and all subsamples were referenced to the stratigraphy of core TKS I. We thus obtained a total of 20 U–Th dates on a common depth axis (Fig. 4; Table 1). The 2 sigma errors range from 0.7% to 4.3% but are typically close to 2% at ca 120 ka. Correction for detrital Th was small for most samples (typically within a few hundred years). The age model is derived by a sigmoidal function (3-parameter sigmoid, Fig. 4). According to this age model deposition of the white translucent inclusion-poor calcite started at  $126.1 \pm 1.0$  ka (near base) and subsamples of the following ca 18 cm yielded ages undistinguishable within the 2 sigma error from the basal age. The pronounced 4‰ drop in  $\delta^{18}\text{O}$  commenced at ca 119 ka and U–Th ages for the following 2 cm of laminated calcite become successively younger until hiatus H1.

U–Th dates of the brown calcite sequence (not shown) are compromised by detrital Th and the very large correction resulted in ages with large uncertainties. The isotopic dates are in stratigraphic order, however, and indicate repeated deposition of brown calcite during MIS 5a (i.e. between H1 and H2) and MIS 3 (above H2), respectively (Fig. 4).

The ENT 10 flowstone yielded two preliminary U–Th ages of  $118.2 \pm 2.5$  ka at 20 mm and  $121.4 \pm 1.9$  ka at 68 mm from top, which are consistent with the proposed correlation with the TKS record based on the  $\delta^{18}\text{O}$  profile (Table 1; Fig. 4).

## 5. Discussion

### 5.1. Temperature precipitation and seasonality changes at the end of MIS 5e

Speleothems are an archive of paleogroundwater that is controlled primarily by climate. Unfortunately, this seemingly simple relationship may be masked by other processes, such as soil dynamics, (epi)karst hydrology, cave ventilation and evaporation (Tooth and Fairchild, 2003; Spötl et al., 2005; Fairchild et al., 2006; Asrat et al., 2007). In order to fully exploit the potential of speleothems as paleoenvironmental archives it is therefore essential to carefully assess proxy-climate relationships and—in the case of stable isotopes—to evaluate equilibrium conditions during speleothem growth (e.g., Mickler et al., 2004, 2006).

#### 5.1.1. Modern proxy calibration: $\delta^{18}\text{O}$ meteoric precipitation

Drip water in Entrische Kirche cave originates from meteoric precipitation falling in the small catchment some 800 m above and to the east of the cave. In the Alps the  $\delta^{18}\text{O}$  value of meteoric precipitation ( $\delta^{18}\text{O}_{\text{ppt}}$ )—ultimately recorded by the isotopic composition of speleothems—is controlled by climate in two ways: (a)  $\delta^{18}\text{O}_{\text{ppt}}$  increases as a function of increasing air temperature and the empirically

determined gradient is close to  $0.6\text{‰}/\text{°C}$  (Rozanski et al., 1992; Humer, 1995); and (b)  $\delta^{18}\text{O}_{\text{ppt}}$  decreases with increasing altitude at a rate of typically  $-0.15\text{‰}/100$  m, although there are regional differences (Humer, 1995; Schotterer et al., 1997; Schürch et al., 2003). In order to examine the intraannual  $\delta^{18}\text{O}_{\text{ppt}}$  variability data from meteorological stations at Böckstein and Obertauern, located within 20 and 35 km of Entrische Kirche cave, respectively, were used (Fig. 1). The composite record based on weighted monthly  $\delta^{18}\text{O}$  data from both stations was adjusted to the mean altitude of the cave's infiltration area (1900 m) by applying an altitude effect of  $-0.15$  ( $\pm 0.02$ )‰/100 m and mean  $\delta^{18}\text{O}_{\text{ppt}}$  values for summer (May–October) and winter (November–April) were calculated. Summer precipitation in the catchment area of the Entrische Kirche cave consequently accounts for 63% of the annual precipitation (mean  $-11.0\text{‰}$ ), whereas the winter season contributes 37% (mean  $-17.3\text{‰}$ ). Mixing these two components in the karst aquifer gives rise to a hypothetical groundwater  $\delta^{18}\text{O}$  value of  $-13.3$  ( $\pm 0.8$ )‰, which is within the range of measured seepage waters in Entrische Kirche cave (see below).

#### 5.1.2. Evaluating isotopic equilibrium in today's cave

The stable oxygen isotope composition of actively forming flowstones from Entrische Kirche cave is  $-10.2$  ( $\pm 0.4$ )‰ (Table 2b). Water samples collected bimonthly at several drip sites within the Entrische Kirche cave show average  $\delta^{18}\text{O}$  values of  $-12.8$  ( $\pm 0.3$ )‰ (Table 2a). Using the Friedman and O'Neil (1977) relationship these parameters yield an equilibrium temperature of  $5.1$  °C ( $2.4$ – $7.9$  °C using the standard deviations of the input data), indistinguishable from the modern interior cave temperature of  $5.5$  °C suggesting isotopic equilibrium during flowstone formation. This is consistent with measurements showing negligible evaporation in the

Table 2

Isotopic composition of modern water and speleothem calcite in the Entrische Kirche cave

(a) $\delta^{18}\text{O}$ cave water (‰, VSMOW)					
Cave stream	Rechter Schlot	Zweite Etage	Kreuz	Nilpferd-maul	TK Schlot
	–12.70	–12.58	–12.64	–12.87	–12.81
	Mean: –12.81				
	S.D.: 0.33				
(b) $\delta^{18}\text{O}$ active flowstone (‰, VPDB)					
ENT 12	ENT 13	ENT 14	ENT 15		
–10.28	–10.28	–9.50	–10.16		
	Mean: –10.15				
	S.D.: 0.38				

Values given for individual sites are based on several analyses each.

interior of the cave where these speleothems are forming today.

In essence, calcite precipitates in today's Entrische Kirche cave is close to isotopic equilibrium and records the isotopic composition of meteoric precipitation that infiltrates at ca 1900 m.

### 5.1.3. Last Interglacial calcite: isotope systematics

Isotopic equilibrium is generally regarded as a prerequisite for reliable paleoclimatic interpretations of speleothem stable isotope data (e.g., McDermott et al., 2005). While well established tests can be used to assess equilibrium conditions in stalagmites (Hendy, 1971; Mickler et al., 2006; Wiedner et al., 2008), surprisingly little systematic work has been performed on flowstones. Taking samples along growth layers, a task already difficult in stalagmites lacking clearly visible layering, is even more challenging in the case of flowstones, where multiple sources of drip or splash water may give rise to complex growth morphologies and locally also laterally extensive formations. Sampling a flowstone showing a simple radial growth shape (sourced from a single point) would still be a nontrivial task, as a series of drill cores taken radially along flow paths are required and individual growth layers must be unambiguously traced across these cores. Not least because of cave conservation issues we opted for a different approach and took four drill cores of the TKS flowstone to evaluate the internal consistency of the isotope signal analysed continuously along these cores.

A qualitative intercomparison of three TKS cores analysed for their stable isotopic composition shows a very high degree of consistency in both the  $\delta^{13}\text{C}$  and  $\delta^{18}\text{O}$  values and a good fit with the shorter ENT 10 record (Fig. 4). This is particularly true for the first-order trend, e.g. the ramp-like increase in  $\delta^{18}\text{O}$  values in the Last Interglacial section and the subsequent isotopic shift towards much lower values. As these trends are also mirrored by flowstone ENT 10 we argue that they are more likely reflecting a climate signal rather than features specific to individual speleothem depositional sites.

As classical 'Hendy tests' cannot be performed on these drill cores the degree of correlation between the  $\delta^{13}\text{C}$  and  $\delta^{18}\text{O}$  curves is used to qualitatively assess the relative importance of equilibrium versus kinetic fractionation during calcite precipitation. Inspection of the first-order trend of the white calcite succession reveals that  $\delta^{13}\text{C}$  and  $\delta^{18}\text{O}$  are essentially uncorrelated during the Last Interglacial:  $\delta^{13}\text{C}$  shows several highs and lows which can be traced throughout all TKS cores, while  $\delta^{18}\text{O}$  values increase rather monotonously when plotted on a depth scale (Fig. 5). Detrending the curves allows to examine the degree of correlation at the higher frequency variability which amounts up to ca 1.6‰ in  $\delta^{18}\text{O}$  and about twice as much in  $\delta^{13}\text{C}$  (Fig. 5). At this high frequency both isotopes are highly correlated and the slope of ca 0.91 (Fig. 5) suggests kinetically controlled fractionation (Mickler et al., 2006; Wiedner et al., 2008). We therefore

argue that second-order variability seen in the TKS data is likely to be a kinetic signal (though the underlying forcing may still be a climatic one), whereas we see no reason to question the climatic control of the first-order trend in  $\delta^{18}\text{O}$ , which we draw along the minima of the  $\delta^{18}\text{O}$  values (Fig. 4).

### 5.1.4. The end of the Last Interglacial: evaluating isotope changes

The most striking feature is the large drop in  $\delta^{18}\text{O}$  at the end of the interglacial seen in all three TKS cores as well as in the ENT 10 sample (Fig. 4). Although individual  $\delta^{18}\text{O}$  values reach as high as  $-7.9\text{‰}$  in the uppermost Last Interglacial calcite we took a conservative value of  $-9.5\text{‰}$  for the onset of this decrease as we argued above that up to 1.6‰ of the variability in the  $\delta^{18}\text{O}$  data is due to kinetic fractionation. Close inspection reveals that the amplitude and relative length of the high-frequency cycles on the Last Interglacial "ramp" are variable among the four samples, whereas the isotope minima in the upper part of the "ramp" are rather consistent and close to  $-9.5\text{‰}$  (Fig. 4). We regard this value as the best estimate of calcite precipitated close to isotopic equilibrium at the end of the Last Interglacial. As the minimum value following the drop is  $-12.4\text{‰}$  (average of the four records) the total decrease at the end of the Last Interglacial amounts to ca 2.9‰. Petrography strongly suggests that calcite deposition was continuous from the Last Interglacial until hiatus H1, i.e. the entire isotope shift of ca 2.9‰ occurred during deposition of inclusion-poor, white calcite (see below).

There are currently no data available from continuous climate archives on the European continent that recorded the Lastglacial inception using oxygen isotopes. It is therefore instructive to look at other intervals within the Lastglacial–Interglacial cycle for a comparison. Studies of paleogroundwaters in Switzerland, southern Germany and Austria showed a 2.5–3‰ change at Termination I (Beyerle et al., 1998; Darling et al., 2006). A very similar isotope shift was recorded between the Allerød and the Younger Dryas in Bavarian lake sediments (ca 3‰; von Grafenstein et al., 1999) and speleothems (2.5–3‰; Wurth et al., 2004; Spötl, unpublished data). Finally, speleothem data from Spannagel Cave indicate a ca 2.5‰ amplitude between stadials and interstadials during MIS 3 (Spötl et al., 2006). Qualitatively speaking, the 2.9‰ drop recorded in our flowstone samples thus appears to be a reasonable figure for a major climatic change in the alpine realm (the MIS 5e/d transition).

Higher  $\delta^{18}\text{O}$  values in the Last Interglacial portion of the TKS record compared to those from modern flowstones in Entrische Kirche cave ( $-9.5\text{‰}$  versus  $-10.2\text{‰}$ ) qualitatively suggest that the former was warmer than today. Using present-day isotope systematics a 1 °C increase of the MAAT would lead to a 0.59 ( $\pm 0.08$ )‰ increase in  $\delta^{18}\text{O}$  of precipitation (Rozanski et al., 1992), which is indistinguishable from the temperature gradient measured at the nearby meteorological station Böckstein (0.56‰/°C;

Humer, 1995). This warming would inevitably propagate into the cave's interior and fractionation during calcite precipitation would partially offset the atmospheric temperature effect ( $-0.24\text{‰}/^{\circ}\text{C}$ ; Friedman and O'Neil, 1977). Hence, warming (cooling) by  $1^{\circ}\text{C}$  is expected to result in an increase (decrease) in  $\delta^{18}\text{O}$  of cave calcite of  $0.35 (\pm 0.08)\text{‰}$ . This relationship suggests that the MAAT during the Last Interglacial was higher than today by  $2.0 (\pm 0.6)^{\circ}\text{C}$ , which is at least partially consistent with estimates of the summer temperature on the northern fringe of the Alps based on pollen transfer functions (ca  $2^{\circ}\text{C}$  warmer than today; Klotz et al., 2004). Conversely, the interior cave temperature was  $7.5 (\pm 0.6)^{\circ}\text{C}$  at that time (up from  $5.5^{\circ}\text{C}$  today).

The MIS 5e/d transition resulted in a major drop in global sea level. Current estimates range from  $-25\text{ m}$  to as much as  $-70\text{ m}$  relative to the MIS 5e sea level (Lambeck and Chappell, 2001; Lea et al., 2002; Waelbroeck et al., 2002; Siddall et al., 2003), which translates into an increase in the  $\delta^{18}\text{O}$  of deep ocean water of ca  $0.2\text{--}0.6\text{‰}$  (Duplessy et al., 2007). With respect to the  $\delta^{18}\text{O}_{\text{ppt}}$  signal ultimately recorded in our speleothems, however, changes in the  $\delta^{18}\text{O}$  value of the (Atlantic) surface waters are of much greater relevance as they are the moisture source for precipitation in the Alps. We use recently published data from Skinner and Shackleton (2006) to estimate this effect for our cave site. These authors reported a ca  $1\text{‰}$  change in the  $\delta^{18}\text{O}$  of the deep water associated with a ca  $2\text{‰}$  change in the  $\delta^{18}\text{O}$  value of the surface water in the Northeast Atlantic during Terminations I and II. Using these figures as a guide we infer that the  $\delta^{18}\text{O}$  value of the surface water became ca  $0.4\text{--}1.2\text{‰}$  higher during the MIS5e/d transition (equivalent to a sea-level drop of  $-25$  to  $-70\text{ m}$ , see above). We adopted a conservative value of  $0.6\text{‰}$  (equivalent to ca  $-36\text{ m}$  of sea-level drop) in order to correct the measured isotope shift in our speleothems for isotopic changes of the moisture source. We are aware that this is a first-order approximation only and does not take into account e.g. isotopic effects as a result of changing trajectories (which await a new generation of high-resolution climate models including isotopes). As a first approximation the resultant shift of  $3.5\text{‰}$  in the flowstone record subsequent to the end of the Last Interglacial translates into ca  $8.1\text{--}12.9^{\circ}\text{C}$  (mean  $10.0^{\circ}\text{C}$ ) of atmospheric cooling, under the assumption that the temperature change was uniform throughout the year (i.e. equal summer and winter cooling).

To sum up, oxygen isotope data record a dramatic temperature drop at the end of the Last Interglacial at Entrische Kirche, consistent with the general view of glacial inception at that time (ca  $118\text{ ka}$ ).

#### 5.1.5. The end of the Last Interglacial: cave freezing and (peri)glacial processes

Cooling by ca  $10^{\circ}\text{C}$ , as deduced from the stable oxygen isotope record, would bring the interior cave temperature well below the freezing point (starting from  $7.5^{\circ}\text{C}$  during the Last Interglacial, see above) and as a consequence

calcite deposition would cease. This scenario is incompatible with petrographic evidence showing uninterrupted speleothem growth for ca  $4\text{ ka}$  subsequent to the isotope drop. Equally important, epifluorescence microscopy shows that the karst hydrology and probably also the soil composition above the cave did not change significantly during this period of time (but only subsequent to hiatus H1). Central to this scenario is the assumption that cooling is distributed equally throughout the year (i.e. summer and winter are equally affected). Attributing the isotopic shift at the end of the Last Interglacial solely to temperature would inevitably cause cave freezing (the interior cave temperature would fall to  $-0.6$  to  $-5.4^{\circ}\text{C}$  using minimum and maximum estimates, respectively). We therefore conclude that uniform cooling likely overestimates the magnitude of this climate change.

The MAAT in the catchment above the cave ( $1800\text{--}2100\text{ m}$ ) is currently ca  $+1^{\circ}\text{C}$  and was probably  $+3.1 (\pm 0.6)^{\circ}\text{C}$  during the Last Interglacial (see above). Cooling by ca  $10^{\circ}\text{C}$  would cause the MAAT in the catchment to fall to ca  $-7^{\circ}\text{C}$ . Snow and ice would accumulate there and deposition of clean spelean calcite containing fluorescent organic constituents (derived from the soil zone, SOM 1) would come to an end. We thus identify a glacial threshold—ca  $0^{\circ}\text{C}$  at  $1100\text{ m}$ , equivalent to  $-5^{\circ}\text{C}$  at  $1900\text{ m}$ —for this cave system below which calcite deposition is exposed to cease and water in the cave fissure aquifer freezes.

In addition, periglacial processes in the catchment area will intensify as a result of progressive cooling and in particular due to the development of discontinuous permafrost. In the Alps the  $-1^{\circ}\text{C}$  MAAT isotherm coincides with the onset of discontinuous permafrost giving rise to an increased flux of fine-grained detrital material into the karst system due to the disintegration of the vegetation cover and solifluction processes (Haeberli, 1982, 1983; Jaesche, 1999; Veit, 2002). As a consequence we anticipate precipitation of clean spelean calcite to slow down and to be eventually superseded by intermittent growth of calcite containing fine-grained detritus.

As the features observed in the TKS and the ENT 10 samples (white clean calcite with occasional UV lamination deposited over several thousands of years subsequent to the major isotope shift) are not consistent with periglacial activity this corroborates our previous conclusion that the quantitative interpretation of the observed isotope shift requires refinement.

#### 5.1.6. The end of the Last Interglacial: introducing seasonality

In order to reconcile speleothem deposition with the isotopic evidence of strong cooling we will now abandon the simple assumption of uniform cooling and consider seasonality effects. Recently, Denton et al. (2005) drew attention to the role of seasonality during climate change and emphasized that cooling during the Younger Dryas stadial was principally a winter phenomenon, with no

substantial change in summer temperatures except the length of the growing season. Widespread freezing of the North Atlantic surface water is the most likely explanation for the drastic increase in continentality in central Europe during cold intervals (Alley, 2000; Broecker, 2006). Global-scale model simulations of the Lastglacial inception, however, draw a somewhat different picture emphasizing meridional and interbasin changes in the atmospheric freshwater transport (Gröger et al., 2007), complex ocean–atmosphere linkages as well as strong vegetation and snow-albedo feedbacks (e.g., Khodri et al., 2001; Calov et al., 2005a, b) with high precipitation rates over high northern latitudes. There, precipitation is mainly delivered as winter snow and consequently these models predict gradually expanding ice caps around 117–118 ka (Khodri et al., 2001, 2003; Calov et al., 2005a; Cane et al., 2006).

In order to test and quantify the role of seasonality changes during the Lastglacial inception in the Alps, we developed a simple modelling approach constrained by the oxygen isotope data of our speleothem samples. Starting point of this model is the intraannual  $\delta^{18}\text{O}_{\text{ppt}}$  variability obtained from the meteorological stations at Böckstein and Obertauern (Fig. 1) and the assumption that present-day isotope systematics applied to Last Interglacial conditions.

#### 5.1.7. The seasonality model: calibration and performance for MIS 5e conditions

As discussed above, oxygen isotope data of the MIS 5e calcite suggest warmer conditions during the Last Interglacial by up to 2 ( $\pm 0.6$ ) °C. In order to model seasonality changes during the MIS 5e/d transition we first adjusted the value of modern  $\delta^{18}\text{O}_{\text{ppt}}$  ( $-13.3 \pm 0.3\text{‰}$  in the catchment area at a mean elevation of 1900 m) to the conditions of the Last Interglacial. Taking into account uncertainties associated with modern  $\delta^{18}\text{O}_{\text{ppt}}$  and estimates of the MAAT during MIS 5e and the atmospheric temperature effect ( $0.59 \pm 0.08\text{‰}$ ) we obtained a  $\delta^{18}\text{O}_{\text{ppt}}$  value of  $-12.1 (\pm 0.9)\text{‰}$  for MIS 5e precipitation at 1900 m. We cross-checked this value by computing the temperature of calcite precipitation during MIS 5e using the relationship of Friedman and O'Neil (1977): Last Interglacial calcite ( $\delta^{18}\text{O} = -9.5\text{‰}$ , see above and Table 3) is in isotopic equilibrium with the inferred  $\delta^{18}\text{O}_{\text{ppt}}$  value of  $-12.1 (\pm 0.9)\text{‰}$  at a cave air temperature of  $+5.1 \text{ °C}$  ( $+1.6$  to  $+8.7 \text{ °C}$  using the standard deviation of  $\delta^{18}\text{O}_{\text{ppt}}$ ), well within the range anticipated for the Last Interglacial ( $7.5 \pm 0.6 \text{ °C}$ , see above and Table 3).

Starting from present-day isotope systematics it thus appears that we can reliably adjust and transfer modern isotope parameters to climate conditions during MIS 5e. Accordingly, and under the assumption that the pattern of seasonal  $\delta^{18}\text{O}_{\text{ppt}}$  variation during the Last Interglacial was broadly similar to today, winter precipitation had a mean  $\delta^{18}\text{O}$  value of  $-16.1\text{‰}$  (accounting for 37% of the MAP), whereas the summer  $\delta^{18}\text{O}_{\text{ppt}}$  value averaged  $-9.8\text{‰}$  (63% of the MAP).

#### 5.1.8. The seasonality model: setup for MIS 5d conditions

The model is based on the empirically established relationship between temperature and  $\delta^{18}\text{O}_{\text{ppt}}$  as calculated for continental Europe by Rozanski et al. (1992). In order to model different seasonality effects we varied the  $\delta^{18}\text{O}_{\text{ppt}}$  value and thus the isotopic composition of the drip water seasonally. Using an updated database (Global Network of Isotopes in Precipitation, 1960–2001) we calculated gradients for winter (November–April) and summer (May–October) of 0.66 and 0.47‰/°C, respectively. The annual gradient is 0.59‰/°C, i.e. identical to Rozanski et al. (1992); (Table 3). As outlined in the previous section we started with  $\delta^{18}\text{O}_{\text{ppt}}$  values of  $-16.1\text{‰}$  and  $-9.8\text{‰}$  for MIS 5e winters and summers, respectively (Table 3). By varying these values systematically using the seasonal isotope temperature coefficients, we modelled different cooling scenarios for the end of the Last Interglacial. Changing the relative proportions of winter and summer precipitation (37:63% today—incorporated into the model as weighting factors of  $\delta^{18}\text{O}_{\text{ppt}}$ ) allows us to further investigate the effect of dryer and wetter climate for both seasons on a relative scale. Details about the parameter settings for this model are provided in Table 3 and the results are shown in Fig. 6.

As a next step we identified combinations of temperature and drip water isotope values which result in the precipitation of calcite with a  $\delta^{18}\text{O}$  value of  $-12.4\text{‰}$  (using Friedman and O'Neil, 1977), i.e. the  $\delta^{18}\text{O}$  value of the laminated white calcite deposited during MIS 5d. Taking into account uncertainties associated with the estimated cave air temperature ( $\pm 0.6 \text{ °C}$ ) we defined an array in a  $\delta^{18}\text{O}_{\text{ppt}}$  versus temperature diagram which represents the most likely field of the calcite precipitation during MIS 5d (Fig. 6).

In the case of no change in seasonality (uniform cooling) and applying an annual coefficient of 0.59‰/°C (Fig. 6, scenario 0)  $\delta^{18}\text{O}_{\text{ppt}}$  values decrease from MIS 5e levels ( $-12.1\text{‰}$  and  $7.5 \text{ °C}$ ) to freezing conditions ( $-2 \text{ °C}$  at 1100 m, i.e. inside the cave). This confirms our previous findings that uniform cooling throughout the year cannot account for the observed isotopic composition of calcite formed during MIS 5d. Several studies have demonstrated, however, that the assumption of invariant isotope-temperature gradients through time is invalid. Paleotemperature reconstructions from the Greenland ice sheet based on bore-hole temperature measurements (Dahl-Jensen et al., 1998; Cuffey and Marshall, 2000) and on gas-phase isotopic compositions (Severinghaus et al., 1998) revealed a significantly smaller gradient for the last deglaciation (0.33‰/°C). This reduction in the slope can be related to a combination of source temperature changes and changes in the annual distribution of precipitation (Huber et al., 2006). No reliable data are currently available for central Europe, although a paleogroundwater study from Switzerland suggested a gradient for the last deglaciation similar to today's ( $0.47 \pm 0.17 \text{ °C}$ ; Beyerle et al., 1998). Uniform cooling using these two lower gradients actually results in even larger discrepancies between the

Table 3

Parameters used in the isotopic seasonality model. MAAT: mean annual air temperature

---

*Isotope–temperature coefficients*

Annual mean:  $0.59 \pm 0.08\text{‰}/^{\circ}\text{C}$  (Rozanski et al., 1992)

Winter (November–April):  $0.66 \pm 0.08\text{‰}/^{\circ}\text{C}$  (see supplement 2)

Summer (May–October):  $0.47 \pm 0.08\text{‰}/^{\circ}\text{C}$  (see supplement 2)

*Altitude effect*  $0.15 \pm 0.02\text{‰}/100\text{ m}$

*Modern parameters*

$\delta^{18}\text{O}$  of precipitation in catchment (1900 m a.s.l.)

Annual mean:  $-13.3 \pm 0.3\text{‰}$  VSMOW

Winter (November–April):  $-17.3 \pm 0.08\text{‰}$  VSMOW

Summer (May–October):  $-11.0 \pm 0.08\text{‰}$  VSMOW

Cave air and MAAT (1100 m a.s.l.):  $5.5^{\circ}\text{C}$

MAAT in catchment (1900 m a.s.l.):  $1.1^{\circ}\text{C}$

$\delta^{18}\text{O}$  calcite (flowstones):  $-10.15 \pm 0.38\text{‰}$  VPDB

*Last interglacial parameters and adjustments*

$\delta^{18}\text{O}$  precipitation in catchment (1900 m a.s.l.)

Annual mean:  $-12.1 \pm 0.9\text{‰}$  VSMOW

Winter (November–April):  $-16.1 \pm 0.08\text{‰}$  VSMOW

Summer (May–October):  $-9.8 \pm 0.08\text{‰}$  VSMOW

Cave air and MAAT (1100 m a.s.l.):  $7.5 \pm 0.6^{\circ}\text{C}$

MAAT in catchment (1900 m a.s.l.):  $3.1 \pm 0.6^{\circ}\text{C}$

$\delta^{18}\text{O}$  of MIS 5e calcite:  $-9.5 \pm 0.08\text{‰}$  VPDB

$\delta^{18}\text{O}$  of MIS 5d calcite:  $-12.4 \pm 0.08\text{‰}$  VPDB

---

isotopic composition of MIS 5d calcite and modelled  $\delta^{18}\text{O}_{\text{ppt}}$ –temperature combinations (Fig. 6, *scenario 0*). We therefore continue to use the empirically determined modern gradient of  $0.59\text{‰}/^{\circ}\text{C}$  in all subsequent calculations.

#### 5.1.9. The seasonality model: applied to MIS 5d conditions

We examined six different climate scenarios for MIS 5d by varying the extent of winter versus summer cooling and drying, respectively (Fig. 6). *Scenario 1* invokes cooling and drying of the winter only, whereas *scenarios 2, 3* and *4* model differential summer cooling and drying in addition to winter cooling and drying. Finally, we evaluate the effect of increased winter precipitation combined with differential cooling and investigate the consequences of changes in the duration of the cold season (*scenarios 5* and *6*).

*Scenario 1*: Summer temperature and  $\delta^{18}\text{O}_{\text{ppt}}$  are kept constant (i.e. at MIS 5e conditions) and the winter is progressively cooled at  $2^{\circ}\text{C}$  intervals from  $0$  to  $-20^{\circ}\text{C}$  giving rise to an annual cooling of  $0$  to  $-10^{\circ}\text{C}$ . Winter drying progresses from  $0\%$  to  $50\%$ . The  $\delta^{18}\text{O}_{\text{ppt}}$  values range from  $-11.3\text{‰}$  to  $-17.0\text{‰}$  and are incompatible with the measured MIS 5d calcite composition.

*Scenario 2* adds the effect of a cooler summer. We allow summer cooling to be  $50\%$  that of the winter cooling. The  $\delta^{18}\text{O}_{\text{ppt}}$  values range from  $-11.2\text{‰}$  to  $-17.4\text{‰}$  but again do not intersect the MIS 5d calcite field (Fig. 6).

In *scenarios 3* and *4* the winter is cooled in the same manner as before and winter precipitation is reduced by  $20\%$  (*scenario 3*) and  $40\%$  (*scenario 4*), respectively. The summer cools only slightly ( $20\%$  of winter cooling), but its precipitation is reduced strongly between  $10\%$  and  $70\%$ .

Both scenarios result in combinations of  $\delta^{18}\text{O}_{\text{ppt}}$  and temperature that are consistent with the MIS 5d calcite field (Fig. 6): about  $-6$  to  $-8^{\circ}\text{C}$  of winter cooling ( $-1.2$  to  $-1.6^{\circ}\text{C}$  of summer cooling),  $50$ – $60\%$  of summer drying and  $20\%$  of winter drying are required for MIS 5d calcite precipitation in *scenario 3* (solutions that plot within the periglacial field and thus close to the glaciation threshold were discarded, see above). *Scenario 4* shows that  $-6$  to  $-9^{\circ}\text{C}$  of winter cooling ( $-1.2$  to  $-1.8^{\circ}\text{C}$  of summer cooling),  $60$ – $70\%$  of summer drying and  $40\%$  of winter drying are compatible with the MIS 5d calcite composition.

*Scenario 5* explores an alternative way to explain MIS 5d calcite precipitation in this cave. The proportion of winter precipitation is varied at the expense of the summer (expressed as the percentage of net winter wetting), i.e. the MAP is kept constant during glacial inception (Fig. 6). Cooling is biased towards winter cooling in a manner similar to the previous scenarios, i.e. progressive winter cooling from  $0$  to  $-20^{\circ}\text{C}$  and only slight summer cooling which is fixed at  $50\%$  of the winter cooling. The results show that MIS 5d calcite deposition becomes feasible if the proportion of winter to summer precipitation ( $37:63$ ) is shifted only slightly in favour of the winter season (to  $48:52$ ; equivalent to a net increase in winter precipitation of  $30\%$ ) and when winter and summer temperatures are lower by ca  $7$  and  $3.5^{\circ}\text{C}$ , respectively (Fig. 6). Further increasing winter precipitation would require still less cooling, e.g. a  $40$ – $50\%$  wetter winter requires less winter and summer cooling ( $-6$  to  $-5^{\circ}\text{C}$  and  $-3$  to  $-2.5^{\circ}\text{C}$ , respectively) to account for the measured composition of MIS 5d calcite.

Finally, we slightly modified *scenario 5* and allowed for an increase in winter precipitation while the amount of summer rainfall was held constant, which causes the MAP to increase accordingly (*scenario 6*, not shown graphically). Winter wetting has to reach ca  $60\%$ , while moderate cooling of both seasons is required to intersect the MIS 5d calcite field ( $7^{\circ}\text{C}$  winter cooling,  $3.5^{\circ}\text{C}$  summer cooling). The MAP then increases by  $22\%$ ,  $48\%$  of which falls during the winter season and  $52\%$  as summer rain.

We also considered the effect of an increase in the duration of the winter season during the MIS 5e/d transition. All scenarios were recalculated with a winter season lasting for  $8$  months (instead of  $6$ ) and the isotope–temperature winter gradient of  $0.66\text{‰}/^{\circ}\text{C}$  as well as winter cooling were applied to the months October to May (the remaining  $4$  months of summer were treated as in the previous scenarios). The longer winter causes  $\delta^{18}\text{O}_{\text{ppt}}$  values to decrease strongly but also affects the MAAT the same time. Our results show that decreasing temperatures counterbalance this precipitation effect and the results are almost identical to those of the previous scenarios.

#### 5.2. The seasonality model: evaluation of results

Model scenarios involving either cooling and/or drying of the winter only (*scenario 1*) or additional slight summer

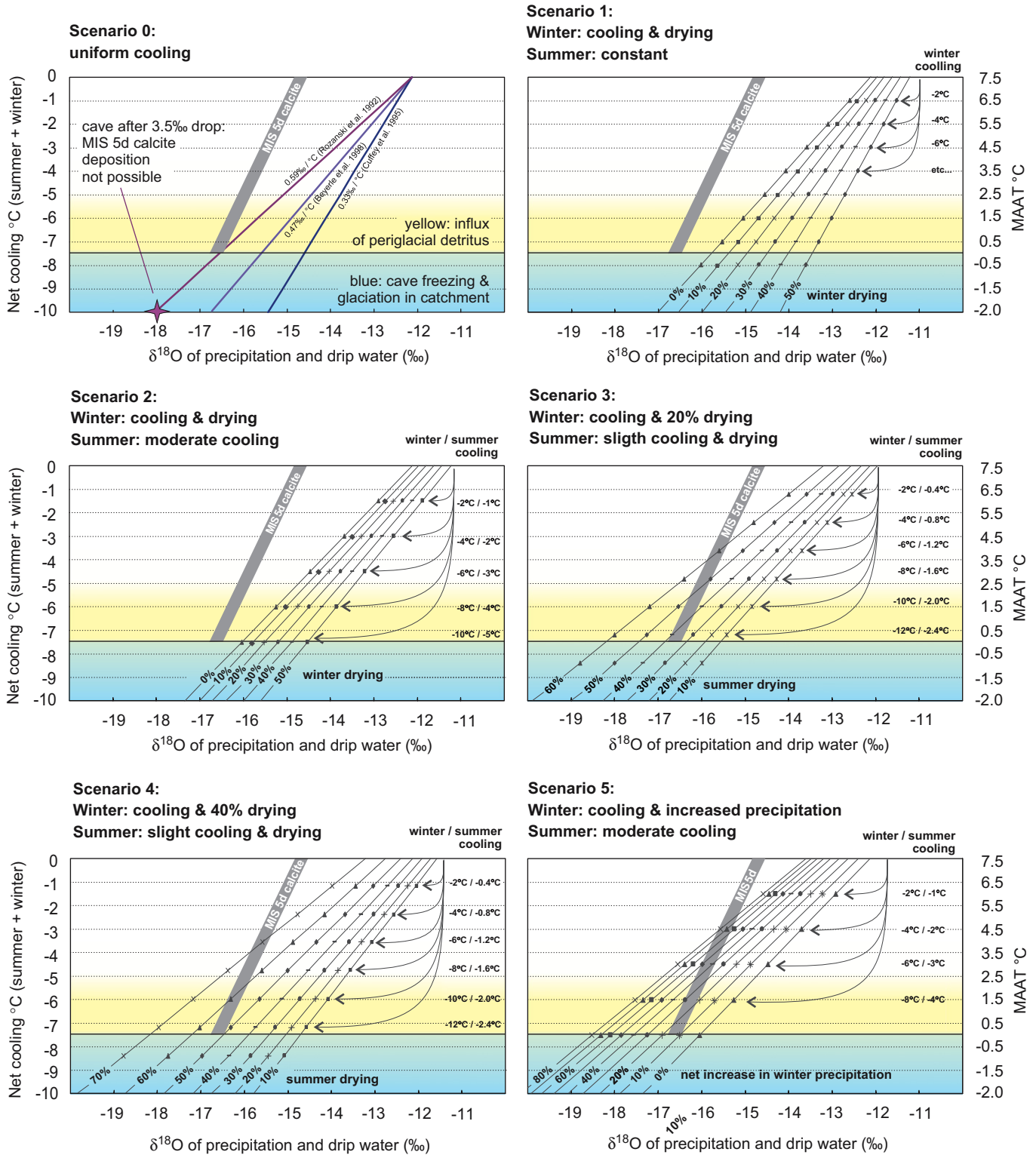


Fig. 6. Results of the isotopic seasonality model. See text for discussion.

cooling (*scenario 2*) are incompatible with  $\delta^{18}\text{O}_{\text{ppt}}$ -temperature combinations required to precipitate MIS 5d calcite. *Scenarios 3* and *4*, however, reveal that the model reacts sensitively to a reduction of the proportion of

summer precipitation. In contrast, the model results are rather insensitive to summer cooling. Scenarios in which summer cooling exceeds winter cooling are not supported by available proxy data from central Europe (e.g. Kühl and

Litt, 2003; Klotz et al., 2004) nor climate model results (e.g. Barron and Pollard, 2002; Cane et al., 2006) and were thus not included in our approach. Indeed, the models require summer temperatures to stay high enough to allow for complete melting of the winter snow pack in order to prevent glaciation of the catchment and freezing of the cave. Temperature and the duration of the warm season are thus limiting parameters in our seasonality model.

From a karst hydrological point of view the summer component of  $\delta^{18}\text{O}_{\text{ppt}}$  dominates the isotopic composition of the drip water, because today more than two thirds of the MAP falls during summer (also assumed to be the case during MIS 5e). Drying the winter relative to the summer thus further increases this bias and makes it more difficult to match the conditions for MIS 5d as constrained by the laminated calcite. Reducing the dominance of isotopically heavy summer precipitation is therefore an important variable, in addition to an increase in winter precipitation. Scenarios 3 and 4 show that if drying is biased toward summer (exceeding winter drying by 20–40%) and if combined with moderate to strong winter (ca  $-6$  to  $-9^\circ\text{C}$ ) and slight summer cooling (ca  $-1$  to  $-2^\circ\text{C}$ ) conditions for MIS 5d calcite precipitation are met. As a result of this, MAP is reduced by 40–50% giving rise to continental climate conditions. These findings are consistent with the reduction of the flowstone growth rate at the end of the Last Interglacial and with uninterrupted deposition of white, detrital-free calcite whose faint fluorescence still suggests vegetation and soil activity in the catchment rather than the development of (peri)glacial conditions.

An alternative solution is suggested by scenarios 5 and 6. Increasing the proportion of winter relative to summer precipitation by 30–60% and cooling both winter and summer ( $-5$  to  $-7^\circ\text{C}$  and  $-2.5$  to  $-3.5^\circ\text{C}$ , respectively) also meets the MIS 5d calcite constraints. This would mean increasing winter precipitation as the regional climate cooled during the glacial inception—conditions generally favourable for glaciation. However, evidence from the Entrische Kirche indicates that altitudes of ca 2000 m still remained well above the glaciation threshold for several millennia.

### 5.3. Model assumptions and additional effects

Our model scenarios are based on the assumption of constancy of seasonal changes in  $\delta^{18}\text{O}_{\text{ppt}}$ , i.e. the intraannual  $\delta^{18}\text{O}_{\text{ppt}}$  variability during MIS 5e was broadly similar to the seasonal  $\delta^{18}\text{O}_{\text{ppt}}$  pattern as determined from nearby meteorological stations. We are unaware of any published datasets constraining the  $\delta^{18}\text{O}_{\text{ppt}}$  parameter for MIS 5e on a seasonal base. Such data would be necessary to improve the accuracy of our model with respect to the MIS 5e starting conditions. Many studies suggest, however, that peak MIS 5e (summer) temperatures were significantly higher than today (e.g., Lozhkin and Anderson, 1995; Cortijo et al., 1999; Vimeux et al., 2002; Klotz et al., 2004;

NGRIP Community Paper, 2004), a fact we also accounted for and which is in agreement with the TKS isotope record (see above). In addition to, or alternatively to higher MIS 5e temperatures an increase in summer precipitation (compared to today) might also have contributed to the higher  $\delta^{18}\text{O}$  values of the MIS 5e section of the TKS record (and thus have influenced the MIS 5e starting position for our model scenarios). As the  $\delta^{18}\text{O}$  values of modern flowstones deviate only by 0.7‰ from the Last Interglacial portion of the TKS record, this change would have had only a minor effect on the large isotope shift at 118 ka.

We also considered possible effects that temperature changes might have had on the isotopic composition of moisture in the vapour source region (i.e. SST changes), which in turn might have influenced the magnitude of the observed isotopic shift at the end of the Last Interglacial. Changes in the source surface water and air temperatures affect the isotopic composition of precipitation via the starting moisture content of an air mass, and due to the effect of temperature on the strongly kinetically controlled fractionation during evaporation. The net effect of these processes is a ca 0.55‰/°C correlation of  $\delta^{18}\text{O}_{\text{ppt}}$  and SSTs in middle and high latitudes (Jouzel et al., 1997 and references therein). For the MIS 5e/d transition SSTs dropped by ca  $3^\circ\text{C}$  in the subpolar North Atlantic (Oppo et al., 2006), by ca  $1^\circ\text{C}$  in the subtropical North Atlantic (Lehman et al., 2002) and by about  $2^\circ\text{C}$  in the western Mediterranean Sea (Martrat et al., 2004; Fig. 7). A recent complex Earth system model suggests ca  $2^\circ\text{C}$  cooling of the Atlantic surface water over the same time interval (Gröger et al., 2007). Assuming a SST change of  $-2^\circ\text{C}$  at the end of the Last Interglacial would thus cause the initial water vapour (and thus the precipitation above the cave site) to increase by 1.1‰ and the measured isotope shift at the MIS 5e/d transition would increase by this amount (from 3.5‰ to 4.6‰). Using the same line of arguments as above the resultant  $\delta^{18}\text{O}$  shift of 4.6‰ translates into ca 10.6–16.9 °C (mean 13.0 °C) of atmospheric cooling above the cave (assuming no seasonal bias). This would inevitably cause cave freezing and speleothem deposition to cease and hence requires refinement (i.e. introduction of seasonality effects as modelled in scenarios 1–6 above).

We also considered the possible southward shifting of the Atlantic vapor source area during glacial inception. Paleoceanographic data suggest that this effect was small, i.e. the subtropical moisture source remained rather stationary (M. Sarnthein, 2007, personal communication) and might have partially offset SST changes discussed above. During cold climate periods, however, today's broad temperate climate belt north of the subtropical Atlantic was reduced to a narrow belt of steeply declining isotherms (Pflaumann et al., 2003). Today, most of the precipitation falling on the Alps ultimately originates in the area of the subtropical Azores High, i.e. at ca 25–35°N from where the moisture is transported toward Europe via westerly and north-westerly winds. This general atmospheric pattern did not change drastically during the MIS

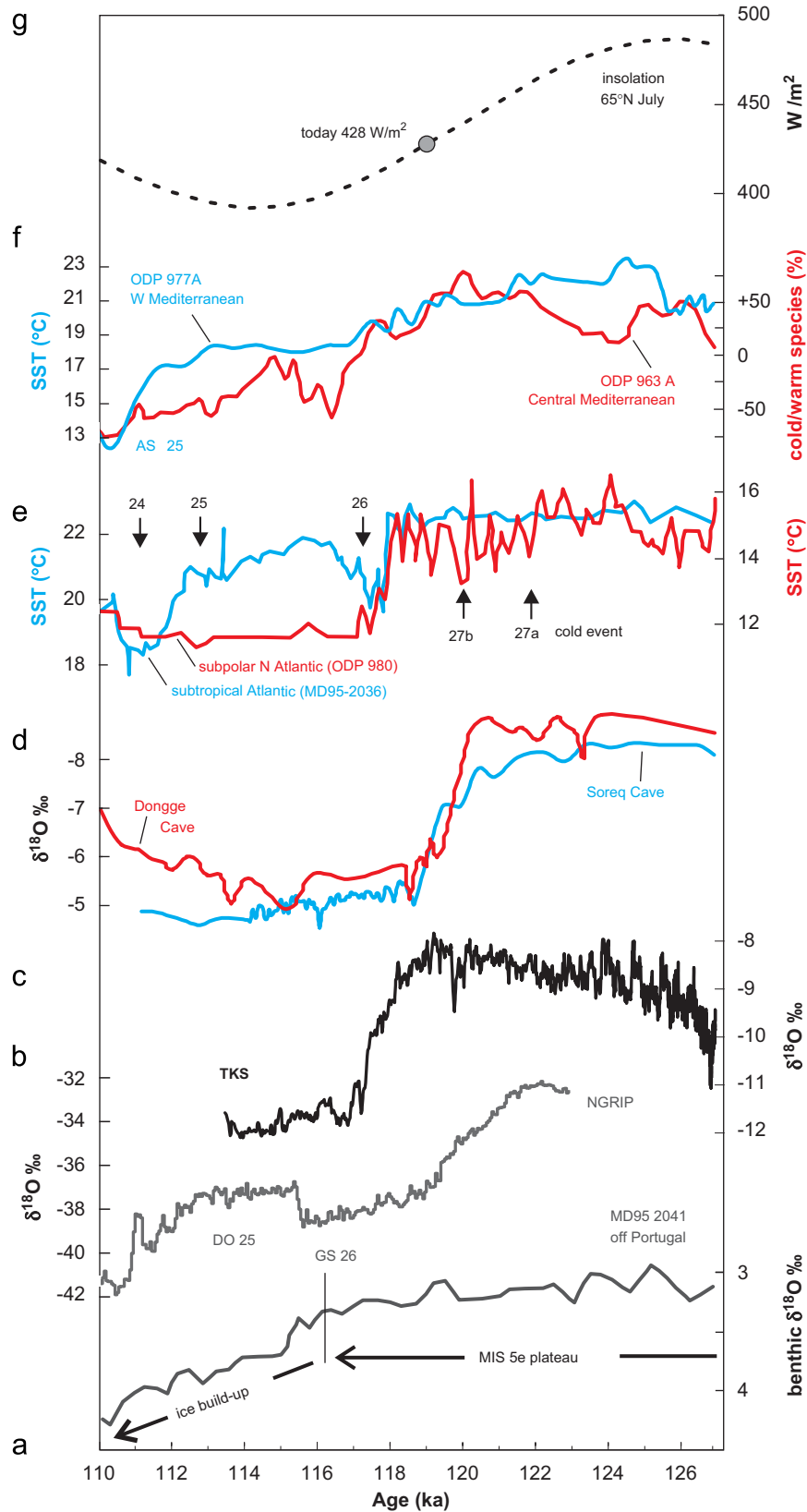


Fig. 7. Correlation of the TKS speleothem with other records plotted on their own time scales. (a) Benthic  $\delta^{18}\text{O}$  record off the coast of Portugal (Shackleton et al., 2003), (b) NGRIP ice core (NGRIP community paper, 2004), (c) TKS stable oxygen isotope record, Entrische Kirche cave, (d) speleothem record from Dongge (Yuan et al., 2004) and Soreq Cave (Bar-Matthews et al., 2003), (e) sea surface temperature from the subpolar (red, Oppo et al., 2006) and the subtropical North Atlantic (blue, Lehman et al., 2002), (f) sea surface temperature of the Alboran Sea (Martrat et al., 2004), percentage of cold and warm water species from the central Mediterranean Sea (Sprovieri et al., 2006), and (g) insolation (Berger and Loutre, 1991). DO: Dansgaard Oeschger event, GS: Greenland stadial. The discrepancy in the U–Th-dated isotopic shifts between the TKS record and the Soreq and Dongge Cave are attributed to age model uncertainties.

5e/d transition. Paleoglaciological observations suggest that only during glacial maxima the N and NW wind (and moisture source) direction was largely replaced by a southerly circulation bringing moist air masses to the southern fringe of the Alps (Florineth and Schlüchter, 2000; Kelly et al., 2004). Air masses picked up moisture from the relatively warm Mediterranean Sea along their trajectories but a significant portion of the moisture was still sourced from the Atlantic.

In summary, and after considering a variety of possible controls on the  $\delta^{18}\text{O}_{\text{ppt}}$  values in the study area we conclude that seasonality changes are the most plausible mechanism to reconcile petrographic (deposition of clean spelean calcite) and isotopic evidence (large drop observed across the MIS 5e/d transition).

#### 5.4. Comparison with proxy records from other archives

This section places the results obtained from the Entrische Kirche speleothem record into the broader paleoclimatic context, in particular with respect to climate changes associated with the MIS 5e/d transition, whereas the isotopic modelling results are discussed in the light of available climate model experiments and records of paleoseasonality in Section 5.5.

Speleothem deposition in the Entrische Kirche started at ca 127 ka, which is consistent within the uncertainties of our age model (ca 2 ka) with the beginning of the marine MIS 5e plateau as identified by benthic  $\delta^{18}\text{O}$  records, e.g. off the coast of Portugal (Shackleton et al., 2002, 2003; Fig. 7a), by the onset of the sea-level highstand dated by corals to  $128 \pm 1$  ka (Stirling et al., 1998), and by the onset of warm and moist interglacial conditions as shown independently by speleothems from Italy ( $129 \pm 1$  ka; Drysdale et al., 2005), Austria (129–130 ka; Spötl et al., 2007), Israel (128–129 ka; Bar-Matthews et al., 2003; Fig. 7d) and China ( $129.3 \pm 0.9$  ka; Yuan et al., 2004; Fig. 7d). Flowstone growth was fast during the first millennia and the  $\delta^{18}\text{O}$  record resolves regular high-frequency cycles of centennial origin, similar to those identified in a stalagmite from the high-alpine Spannagel Cave (Holzkämper et al., 2004), 100 km west of the study area. The regular isotope pattern in the Spannagel speleothem was attributed to solar cycles (Holzkämper et al., 2004) and it is conceivable that high-frequency variability in the Entrische Kirche flowstone was also solar forced, but the uncertainties associated with the age model preclude to test this hypothesis.

Varve-dated German pollen sequences suggests a 2 ka-long climatic optimum from ca 125 to 123 ka (Müller, 1974; Kühl and Litt, 2003) and SST in the North Atlantic (Cortijo et al., 1994; McManus et al., 2002) and on the Iberian margin (Pailler and Bard, 2002) also reached maximum values during this interval. A similar picture emerged from a study of a marine subpolar site, where the climatic optimum lasted until ca 122 ka, terminated by a cold event (no. 27a; Oppo et al., 2006; Fig. 7e). This picture of maximum interglacial warmth between ca 125 and

123 ka is in good agreement with the TKS flowstone which reveals the highest growth rates during this period of time.

In the recent literature, the end of the Last Interglacial appears as a time transgressive and complex sequence of events, depending on the location of the study site and the proxy record used (e.g. Sánchez Goñi et al., 1999, 2005; Kukla et al., 2002; Shackleton et al., 2002, 2003; Müller and Kukla, 2004; Sirocko et al., 2007). Currently, the most accurate and precise time constraints on the end of the Last Interglacial expressed as seen by oxygen isotope data come from speleothems of Israel (119–120 ka; Bar-Matthews et al., 2003), Austria (118–119 ka; Spötl et al., 2007), and China ( $119.6 \pm 0.6$  ka; Yuan et al., 2004; Kelly et al., 2006). Although less well dated, the marine C26 cooling event (ca 118–119 ka) occurred at this time and demonstrates wide-spread cooling of the North Atlantic surface waters from the subpolar region to the subtropics (Adkins et al., 1997; Chapman and Shackleton, 1999; Lehman et al., 2002; Oppo et al., 2006; Fig. 7e). Ice-rafting activity increased during C26 in the eastern subpolar North Atlantic (Oppo et al., 2006) believed to indicate a time when tidewater glaciers first reached the margins of the Nordic Seas (Fronval and Jansen, 1997). Correlation with European pollen records suggests that the North Atlantic Current ceased to penetrate into the Nordic Sea subsequent to the C26 event causing substantial cooling in northern Europe, drier conditions in the Mediterranean region and a southward shift of the polar timberline (Müller and Kukla, 2004; the timing of the C26 event in this study depends on the chosen tie points, but see Drysdale et al. (2007) for precise constraints of these age control points).

The TKS oxygen isotope record suggests a relatively stable climate in the Alps until  $119 \pm 2$  ka, consistent with isotope data from Spannagel Cave (Holzkämper et al., 2005; Spötl et al., 2007). Thereafter  $\delta^{18}\text{O}$  values started to decrease and dropped sharply until  $117 \pm 2$  ka ago. We estimate that the first part of the isotope shift occurred within ca 1.8 ka, whereas the main drop occurred within less than a few centuries only (Fig. 7c). The timing and also the magnitude of this pronounced isotopic shift in the TKS speleothem agrees within dating uncertainties with the end of the Last Interglacial as recorded by Mediterranean and by Chinese stalagmites (Bar-Matthews et al., 2003; Yuan et al., 2004), as well as with the marine C26 event. The timing of the glacial inception as recorded in the TKS flowstone is also in broad agreement with the NGRIP record, although the decrease from Last Interglacial values (–32‰ at ca 122 ka) to the subsequent Greenland stadial 26 (GS 26) suggests a more gradual cooling (Fig. 7b; NGRIP Community Paper, 2004).

Alkenone data suggest a stepwise decrease of west Mediterranean SSTs from 23 to 17 °C starting already at ca 125 ka (Martrat et al., 2004; Fig. 7f). While cold event C26 apparently had no impact on SSTs in the western Mediterranean Sea, C24 is clearly expressed by a SST minimum (Martrat et al., 2004). In contrast, a high-resolution paleoceanographic study from the central

Mediterranean using the abundance of warm and cold water species as a climate proxy (Fig. 7f) suggests punctuated cooling towards the end of the MIS 5e (Sprovieri et al., 2006). This record suggests a first significant climatic event subsequent to the relative warmth of the Last Interglacial at ca 117 ka which might thus be correlated with the isotopic shift in our  $\delta^{18}\text{O}$  curve.

According to the TKS isotope record the climate in the Alps remained rather constant subsequent to the C26 event (cold winters, relatively warm summers, vegetated and stable catchment area at the study site) and until hiatus H1 at ca 114 ka, which marks the end of white, fluorescent calcite deposition (Figs. 3 and 7c). We therefore assign the sudden stop of speleothem growth in the Entrische Kirche cave to the C24 cold event which has been identified throughout the North Atlantic and which had a major impact on the climate of Europe (e.g. Chapman and Shackleton, 1999; McManus et al., 2002; Shackleton et al., 2002). Tree populations in southern Europe, for example, disappeared at that time (Tzedakis, 2003; Müller and Kukla, 2004). Recently, U–Th age constraints on the precise timing of C24 became available (start  $112.0 \pm 0.8$  ka; Drysdale et al., 2007) which are in agreement with our age estimate of hiatus H1 in the TKS flowstone (ca  $114 \pm 2$  ka).

##### 5.5. Seasonality changes during the MIS 5e/d transition: comparison with other proxy data and model results

Continental climate conditions and strong winter cooling suggested by scenarios 3 and 4 are compatible with enhanced seasonality as reconstructed and modelled for stadial–interstadial transitions of the Lastglacial cycle. Alley and Clark (1999) and Alley (2000) showed that the Younger Dryas stadial was most probably caused by widespread freezing of the North Atlantic surface waters in response to a shutdown (or reduction in strength) of the thermohaline conveyor belt. Such abrupt cooling events are now thought to be mainly a winter phenomenon dominated by large changes in winter temperature and propagated by the atmosphere into the trade-wind belt, thus causing a drastic increase in continentality in central Europe during cold intervals (Alley, 2000; Denton et al., 2005; Broecker, 2006). High-resolution climate simulations for interstadial–stadial transitions during the MIS 3 in Europe (Barron and Pollard, 2002) are broadly consistent with this picture and indicate that (1) SSTs and the extent and duration of sea ice in the North Atlantic sector are the most important controlling parameters, (2) a significant reduction in precipitation occurred during MIS 3 stadials which is biased towards the summer season for central Europe, and (3) cooling which is more pronounced during winter than during summer.

Available proxy data from the perialpine region support this view. Quantitative interpretations of fossil pollen assemblages from the northern fringe of the Alps spanning the Last Interglacial–Glacial transition suggest that winter

temperatures dropped ca  $10^\circ\text{C}$  at the end of the Last Interglacial, whereas summer temperatures changed only a little (Klotz et al., 2004; more precisely speaking, the authors reported estimates for the mean temperatures of the coldest and warmest months, respectively). Similar palynological results were reported for other sites in Europe (Kühl and Litt, 2003). Caution is needed in assigning absolute ages to these palynologically derived temperature and seasonality changes as most pollen sequences lack absolute age control. Klotz et al. (2004), for instance, reported an age of ca 114 ka for the end of the Eemian (which is correlative with cold event C24), while Kühl and Litt (2003) constrained the end of the Last Interglacial to ca 117 ka.

Scenarios 5 and 6 of our modelling exercise suggest an alternative way of entering MIS 5d by increasing winter precipitation and allowing for moderate cooling of the winter and summer seasons thus avoiding strong seasonality changes and continentality effects. These model results are in line with a set of sophisticated global-scale model simulations of the Lastglacial inception which emphasize complex ocean–atmosphere linkages (e.g. Khodri et al., 2001, 2003) as well as strong snow–albedo and vegetation feedbacks (e.g. Calov et al., 2005a, b). In all models the decreasing summer insolation causes cooling at high northern latitudes and is considered as the main driving force. Khodri et al. (2001) simulated an increase in atmospheric moisture transport from the equator to the poles, which led to higher precipitation over the high northern latitudes. As a result, snow delivery can increase which in turn causes initiation of gradually expanding ice caps around 117–118 ka (Ruddiman and McIntyre, 1979; Khodri et al., 2001, 2003; Cane et al., 2006). The combination of cooling the high northern latitudes (preventing summer snow melt) and warming the tropical latitudes (enhanced moisture source) is crucial in this model and contrasts to earlier experiments where cooling the atmosphere caused much drier climatic conditions which rendered glacial inception impossible (Vettoretti and Peltier, 2003; Cane et al., 2006). A rapid expansion of the area covered by inland ice in the Northern Hemisphere is starting at about 117 ka in the simulation runs of Calov et al. (2005a, b) and as long as the convection site of the thermohaline circulation is in a northern position, moisture supply and thus ice-build up in high northern latitudes is very effective.

High precipitation rates associated with a cooler climate was also suggested for the MIS 5e/d transition period by studies of European pollen sequences (Guiot et al., 1989; Sánchez Goñi et al., 1999), lake Baikal sediments (Prokopenko et al., 2002), as well as by sediment cores from the subpolar and the subtropical North Atlantic (Cortijo et al., 1994; Adkins et al., 1997; McManus et al., 2002).

Landais et al. (2006) studied the glacial inception as recorded in the NGRIP ice core and examined the interhemispheric sequence of events over this period by placing the NGRIP and Vostok ice cores on a common timescale. They found that after a synchronous north–south temperature decrease (driven by decreasing

insolation in the Northern Hemisphere), the onset of rapid events was triggered in the north by Dansgaard–Oeschger (DO) event 25. Greenland stadial 26 and DO 25 (Fig. 7b) have no Antarctic counterpart, lack ice-rafted detritus and—most importantly—occurred at a time when the atmospheric CO<sub>2</sub> level and the size of the high-latitude ice sheets were still intermediate between interglacial and full glacial values. The authors argued that during glacial inception increased precipitation played a key role and may have caused the thermohaline circulation to become unstable because of too high freshwater input, thus triggering DO event 25. Subsequent DO events show the characteristics of typical full glacial DO events (in terms of amplitude, southern hemisphere reaction and associated ice-rafted detritus in the North Atlantic; Landais et al., 2006). These findings therefore underline the uniqueness of DO 25 and suggest that the chain of processes that operated during the MIS 5e/d transition may not be directly comparable to abrupt stadial–interstadial transitions when the Earth system was in the fully glacial mode. We speculate that the isotope–temperature gradient of 0.59‰/°C (which turned out as a robust estimate for the MIS 5e/d period and rather resembles interglacial values) also points toward this direction as gradients obtained for the last deglaciation (e.g. 0.33‰/°C, Dahl-Jensen et al., 1998; Severinghaus et al., 1998; Cuffey and Marshall, 2000) or Termination I (Beyerle et al., 1998, 0.47‰/°C) are incompatible with our MIS 5d calcite constraints (Fig. 6, scenario 0).

## 6. Conclusions

The termination of the Last Interglacial provides the most recent example of the sequence of events associated with glacial inceptions. U–Th-dated speleothem records, now available from different sites of the Alps, shed new light on the timing of these events and allow testing different paleoclimatic scenarios associated with the demise of the Last Interglacial. Here we demonstrate that climate deteriorated markedly subsequent to ca 119 ka in the Alps, which is consistent with previously published speleothem data from Spannagel Cave (Holzkämper et al., 2005; Spötl et al., 2007). Oxygen isotopes dropped by 3‰ between ca 119 and 117 ka as recorded in a flowstone from Entrische Kirche cave (while no record is available from Spannagel Cave most probably because of its higher elevation and hence lower temperature). Importantly, deposition of white, inclusion-free calcite did not stop at this point but continued until ca 114 ka. We qualitatively interpret this drop in δ<sup>18</sup>O as strong cooling, which, however, was insufficient to cool the cave below freezing. In addition, the fluorescence properties of the white laminated calcite deposited after this drop strongly suggest the presence of at least some vegetation and soil in the catchment area, i.e. no glaciation or intense periglacial processes at elevations of 1800–2200 m during this time period.

In order to quantify the measured shift in δ<sup>18</sup>O in terms of climate variables we use a simple isotopic model calibrated using present-day data (temperature, water and calcite isotopes) and adjusted to MIS 5e starting conditions. Boundary conditions are the freezing point of water (calcite presently forms in this cave at 5.5 °C) and inferred threshold values for the onset of permafrost and/or glaciation in the catchment above the cave. The model shows that the impact of winter δ<sup>18</sup>O<sub>ppt</sub> on the groundwater increased significantly at the MIS 5e/d transition. This rearrangement in the groundwater regime can be achieved in two ways: (a) a highly continental climate with drying biased towards the summer, –6 to –9 °C of winter cooling and summer temperatures not too different to interglacial values, or (b) by a cooler but also much wetter climate whereby precipitation is biased towards the winter (–5 to –7 °C of winter cooling and summer temperatures ca –2.5 to –3.5 °C cooler than during MIS 5e).

General circulation models have recently succeeded in simulating the onset of the Lastglacial by introducing complex ocean–atmosphere and snow–albedo feedbacks (Khodri et al., 2001, 2003; Calov et al., 2005a, b). These models support our model scenarios in which winter precipitation increased and summer and winter seasons cooled only moderately in the Alps during the MIS 5e/d transition, in line with other proxy data (e.g., Adkins et al., 1997; Sánchez Goñi et al., 1999; McManus et al., 2002; Landais et al., 2006). We therefore propose that this speleothem record, which is the first directly dated, continuous stable isotope record of the glacial inception from central Europe, provides useful constraints for future climate models including isotopes.

We thank the federal government of Salzburg for sampling permission in the Entrische Kirche and R. Erlmoser for kind assistance in the cave. Excellent laboratory support was provided by M. Wimmer (Innsbruck) and R. Eichstädter (Heidelberg). R. Boch kindly provided two U–Th dates, C. Mühlinghaus helped with statistical data treatment and M. Sarnthein shared insights into the paleoclimatology of the Atlantic. Two anonymous reviewers are thanked for their constructive comments. This research and M.C.M. were funded by the Austrian Science Fund (FWF, grant Y122-GEO).

## Appendix A. Supplementary Materials

Supplementary data associated with this article can be found in the online version at [doi:10.1016/j.quascirev.2007.11.005](https://doi.org/10.1016/j.quascirev.2007.11.005).

## References

- Adkins, J.F., Boyle, E.A., Keigwin, L., Cortijo, E., 1997. Variability of the North Atlantic thermohaline circulation during the Last Interglacial period. *Nature* 390, 154–156.

- Alley, B.R., 2000. Ice-core evidence of abrupt climate changes. *Proceedings of the National Academie of Sciences of the United States of America*, vol. 97, pp. 1331–1334.
- Alley, B.R., Clark, P.U., 1999. The deglaciation of the Northern Hemisphere: a global perspective. *Annual Review of Earth and Planetary Science* 27, 149–182.
- Asrat, A., Baker, A., Mohammed, M.U., Leng, M.J., Van Calsteren, P., Smith, C., 2007. A high-resolution multi-proxy stalagmite record from Mechara, Southeastern Ethiopia: palaeohydrological implications for speleothem palaeoclimate reconstruction. *Journal of Quaternary Science* 22, 53–63.
- Bar-Matthews, M., Ayalon, A., Gilmour, M., Hawkesworth, C.J., 2003. Sea–land isotopic relationships from planktonic foraminifera and speleothems in the Eastern Mediterranean region and their implications for paleorainfall during interglacial intervals. *Geochimica et Cosmochimica Acta* 67, 3181–3199.
- Barron, E., Pollard, D., 2002. High-resolution climate simulations of oxygen isotope stage 3 in Europe. *Quaternary Research* 58, 296–309.
- Berger, A., Loutre, M.F., 1991. Insolation values for the climate of the last 10 million years. *Quaternary Science Reviews* 10, 297–317.
- Beyerle, U., Purtschert, R., Aeschbach-Hertig, W., Imboden, D.M., Loosli, H.H., Wieler, R., Kipfer, R., 1998. Climate and groundwater recharge during the Last Glaciation in an ice-covered region. *Science* 282, 731–734.
- Brauer, A., Allen, J.R.M., Mingram, J., Dulski, P., Wulf, S., Huntley, B., 2007. Evidence for Last Interglacial chronology and environmental change from southern Europe. *Proceedings of the National Academy of Sciences USA* 104, 450–455.
- Broecker, W.S., 2006. Abrupt climate change revisited. *Global and Planetary Change* 54, 211–215.
- Calov, R., Ganopolski, A., Claussen, M., Petoukhov, V., Greve, R., 2005a. Transient simulation of the last glacial inception. Part I: Glacial inception as a bifurcation in the climate system. *Climate Dynamics* 24, 545–561.
- Calov, R., Ganopolski, A., Claussen, M., Petoukhov, V., Greve, R., 2005b. Transient simulation of last glacial inception. Part II: Sensitivity and feedback analysis. *Climate Dynamics* 24, 562–576.
- Cane, M.A., Braconnot, P., Clement, A., Gildor, H., Joussaume, S., Kageyama, M., Khodri, M., Paillard, D., Tett, S., Zorita, E., 2006. Progress in paleoclimate modelling. *Journal of Climate* 19, 5031–5057.
- Chapman, M.R., Shackleton, N.J., 1999. Global ice-volume fluctuations, North Atlantic ice-rafted events, and deep-ocean circulation changes between 130 and 70 ka. *Geology* 27, 795–798.
- Cheng, H., Edwards, R.L., Hoff, J., Gallup, C.D., Richards, D.A., Asmerom, Y., 2000. The half-lives of uranium-234 and thorium-230. *Chemical Geology* 169, 17–33.
- Cortijo, E., Duplessy, J.-C., Labeyrie, L., Leclaire, H., Duprat, J., vanWeering, T.C.E., 1994. Eemian cooling in the Norwegian Sea and North Atlantic Ocean preceding continental ice-sheet growth. *Nature* 372, 446–449.
- Cortijo, E., Lehman, S., Keigwin, L., Chapman, M., Paillard, D., Labeyrie, L., 1999. Changes in meridional temperature and salinity gradients in the North Atlantic Ocean (30°–72°N) during the Last Interglacial period. *Paleoceanography* 14, 23–33.
- Cuffey, K.M., Marshall, S.J., 2000. Substantial contribution to sea-level rise during the Last Interglacial. *Nature* 404, 591–594.
- Dahl-Jensen, D., Mosegaard, K., Gundestrup, N., Clow, G.D., Johnsen, S.J., Hansen, A.W., Balling, N., 1998. Past temperatures directly from the Greenland Ice Sheet. *Science* 282, 268–271.
- Darling, W.G., Bath, A.H., Gibson, J.J., Rozanski, K., 2006. Isotopes in water. In: Leng, M.J. (Ed.), *Isotopes in Paleoenvironmental Research*. Springer, pp. 1–66.
- Denton, G.H., Alley, R.B., Comer, G.C., Broecker, W.S., 2005. The role of seasonality in abrupt climate change. *Quaternary Science Reviews* 24, 1159–1182.
- Drescher-Schneider, R., 2000. Die Vegetations- und Klimaentwicklung im Riß/Würm-Interglazial und im Früh- und Mittelwürm in der Umgebung von Mondsee. *Ergebnisse der pollenanalytischen Untersuchungen*. In: *Klimaentwicklung im Riß/Würm Interglazial (Eem) und Frühwürm (Sauerstoffisotopenstufe 6-3) in den Ostalpen*. Mitt. Komm. Quartärforsch. Österr. Akad. Wiss., 12, 39–92.
- Drysdale, R.N., Zanchetta, G., Hellstrom, J.C., Fallick, A.E., Zhao, J., 2005. Stalagmite evidence for the onset of the Last Interglacial in southern Europe at  $129 \pm 1$  ka. *Geophysical Research Letters* 32.
- Drysdale, R.N., Zanchetta, G., Hellstrom, J.C., Fallick, A.E., McDonald, J., Cartwright, I., 2007. Stalagmite evidence for the precise timing of N Atlantic cold events during the early last glacial. *Geology* 25, 77–80.
- Duplessy, J.C., Roche, D.M., Kageyama, M., 2007. The deep ocean during the Last Interglacial Period. *Science* 316, 89–91.
- Exner, C., 1979. *Geologie des Salzachtals zwischen Taxenbach und Lend*. Jahrb. Geol. Bundesanstalt, Vienna 122, 1–73.
- Fairchild, I.J., Smith, C.L., Baker, A., Fuller, L.M., Spötl, C., Matthey, D., McDermott, F., 2006. Modification and preservation of environmental signals in speleothems. *Earth-Science Reviews* 75, 105–153.
- Florineth, D., Schlüchter, C., 2000. Alpine evidence for atmospheric circulation patterns in Europe during the Last Glacial Maximum. *Quaternary Research* 54, 295–308.
- Friedman, I., O’Neil, J.R., 1977. Compilation of stable isotope fractionation factors of geochemical interest. In: Fleischer, M. (Ed.), *Data of Geochemistry*, 6th ed. US Geological Survey Prof. Paper, 440-KK, pp. 1–12.
- Fronval, T., Jansen, E., 1997. Eemian and early Weichselian (140–60 ka) paleoceanography and paleoclimate in the Nordic seas with comparisons to Holocene conditions. *Paleoceanography* 12, 443–462.
- Ganahl, P., 1991. Ersatzwasserversorgung für Schwarzach infolge der Staustufe Wallnerau: Österr. Zeitschrift Energiewirtschaft 44, 86–92.
- Grafenstein, U., Erlenkeuser, H., Brauer, A., Jouzel, J., Johnsen, S.J., 1999. A mid-European decadal isotope-climate record from 15,000 to 5000 years B.P. *Science* 284, 1654–1657.
- Gröger, M., Maier-Reimer, E., Mikolajewicz, U., Schurgers, G., Vizcaino, M., Winguth, A., 2007. Changes in the hydrological cycle, ocean circulation, and carbon/nutrient cycling during the last interglacial and glacial transition. *Paleoceanography* 22, PA4205.
- Guiot, J., Pons, A., Beaulieu, L., Reille, M., 1989. A 140 ka continental climate reconstruction from two European pollen records. *Nature* 338, 309–313.
- Haeblerli, W., 1982. Klimarekonstruktion mit Gletscher-Permafrost-Beziehungen. *Materialien zur Physiogeographie* 4, 9–17.
- Haeblerli, W., 1983. Permafrost–glacier relationships in the Swiss Alps today and in the past. In: *Proceedings of the Permafrost: fourth international conference on permafrost*, pp. 415–420.
- Henderson, G.M., 2006. Caving in to new chronologies. *Science* 313, 620–623.
- Hendy, C.H., 1971. The isotopic geochemistry of speleothems. 1. The calculation of the effects of the different modes of formation on the isotopic composition of speleothems and their applicability as palaeoclimatic indicators. *Geochimica et Cosmochimica Acta* 35, 801–824.
- Hoffmann, D.L., Prytulak, J., Richards, D.A., Elliott, T., Coath, C.D., Smart, P.L., Scholz, D., 2007. Procedures for accurate U and Th isotope measurements by high precision MC-ICPMS. *International Journal of Mass Spectrometry* 264, 97–109.
- Holzschläger, S., Mangini, A., Spötl, C., Mudelsee, M., 2004. Timing and progression of the Last Interglacial derived from a high alpine stalagmite. *Geophysical Research Letters* 31, L07201.
- Holzschläger, S., Spötl, C., Mangini, A., 2005. High-precision constraints on timing of Alpine warm periods during the middle to late Pleistocene using speleothem growth periods. *Earth and Planetary Science Letters* 236, 751–764.
- Huber, C., Leuenberger, M., Spahni, R., Flückiger, J., Schwander, J., Stocker, T.F., Johnsen, S., Landais, A., Jouzel, J., 2006. Isotope calibrated Greenland temperature record over Marine Isotope Stage 3 and its relation to CH<sub>4</sub>. *Earth and Planetary Science Letters* 243, 504–519.

- Humer, G., 1995. Niederschlags-Isotopenmeßnetz Österreich. Umweltbundesamt Monographie 52, 1–86.
- Jaesche, P., 1999. Bodenfrost und Solifluktdynamik in einem alpinen Periglazialgebiet (Hohe Tauern, Osttirol). *Bayreuther Geow. Arb.* 20, 1–136.
- Jouzel, J., Alley, R.B., Cuffey, K.M., Dansgaard, W., Grootes, P., Hoffmann, G., Johnsen, S.J., Koster, R.D., Peel, D., Shuman, C.A., Stievenard, M., Stuiver, M., White, W., 1997. Validity of the temperature reconstruction from water isotopes in ice cores. *Journal of Geophysical Research* 102 (C12), 26.471–26.487.
- Kelly, M., Buoncristiani, J.F., Schlüchter, C., 2004. A reconstruction of the LGM ice-surface geometry in the western Swiss Alps and contiguous Alpine regions in Italy and France. *Eclogae Geologicae Helveticae* 97, 57–75.
- Kelly, M.J., Edwards, R.L., Cheng, H., Yuan, D., Cai, Y., Zhang, M., Lin, Y., An, Z., 2006. High resolution characterization of the Asian Monsoon between 146,000 and 99,000 years B.P. from Dongge Cave, China and global correlation of events surrounding Termination II. *Palaeogeography, Palaeoclimatology, Palaeoecology* 236, 20–38.
- Khodri, M., Leclainche, Y., Ramstein, G., Braconnot, P., Marti, O., Cortijo, E., 2001. Simulating the amplification of orbital forcing by ocean feedbacks in the last glaciation. *Nature* 410, 570–574.
- Khodri, M., Ramstein, G., Paillard, D., Duplessy, J.C., Kageyama, M., Ganopolski, A., 2003. Modelling the climate evolution from the Last Interglacial to the start of the last glaciation: the role of Arctic Ocean freshwater budget. *Geophysical Research Letters* 30, 1606.
- Klappacher, W., 1992. Salzburger Höhlenbuch, vol. 5. Salzburg (Landesverein für Höhlenkunde Salzburg), 625pp.
- Klotz, S., Müller, U., Mosbrugger, V., de Beaulieu, J.L., Reille, M., 2004. Eemian and early Würmian climate dynamics: history and pattern of changes in Central Europe. *Palaeogeography, Palaeoclimatology, Palaeoecology* 211, 107–126.
- Kühl, N., Litt, T., 2003. Quantitative time series reconstruction of Eemian temperature at three sites using pollen data. *Veget. Hist. Archaeobot.* 12, 205–214.
- Kukla, G.J., Bender, M.J., deBeaulieu, J.L., Bond, G., Broecker, W.S., Cleveringa, P., Gavin, J.E., Herbert, T.D., Imbrie, J., Jouzel, J., 2002. Last Interglacial climates. *Quaternary Research* 58, 2–13.
- Lambeck, K., Chappell, J., 2001. Sea level change through the Last Glacial Cycle. *Science* 292, 679–686.
- Landais, A., Masson-Delmotte, V., Jouzel, J., Raynaud, D., Johnsen, S., Huber, C., Leuenberger, M., Schwander, J., Minster, B., 2006. The glacial inception as recorded in the NGRIP Greenland ice core: timing, structure and associated abrupt temperature changes. *Climate Dynamics* 26, 273–284.
- Lauscher, F., 1985. Klimatische Synoptik Österreichs mittels der ostalpinen Wetterlagen-klassifikation. *Arbeiten aus der ZAMG*, Vienna, p. 64.
- Lea, D.W., Martin, P.A., Pak, D.K., Spero, H.J., 2002. Reconstructing a 350 ky history of sea level using planktonic Mg/Ca and oxygen isotope records from a Cocos Ridge core. *Quaternary Science Reviews* 21, 283–293.
- Lehman, S.J., Sachs, J.P., Crotwell, A.M., Keigwin, L.D., Boyle, E.A., 2002. Relation of subtropical Atlantic temperature, high-latitude ice rafting, deep water formation, and Europe climate 130,000–60,000 years ago. *Quaternary Science Reviews* 21, 1917–1924.
- Loutre, M.F., Berger, A., 2003. Marine Isotope Stage 11 as an analogue for the present interglacial. *Global and Planetary Change* 36, 209–217.
- Lozhkin, A.V., Anderson, P.M., 1995. The Last Interglaciation in Northeast Siberia. *Quaternary Research* 43, 147–158.
- Martrat, B., Grimalt, J.O., Lopez-Martinez, C., Cacho, I., Sierro, J.F., Flores, A.J., Zahn, R., Canals, M., Curtis, J.H., Hodell, D.A., 2004. Abrupt temperature changes in the Western Mediterranean over the past 250,000 yrs. *Science* 306, 1762–1765.
- McDermott, F., Schwarcz, H., Rowe, P.J., 2005. Isotopes in speleothems. In: Leng, M.J. (Ed.), *Isotopes in Palaeoenvironmental Research*. Springer, Dordrecht, pp. 186–226.
- McManus, J.F., Oppo, D.W., Cullen, J.L., Bond, G.C., 2002. Thermohaline circulation and prolonged interglacial warmth in the north Atlantic. *Quaternary Research* 58, 17–21.
- Mickler, P.J., Banner, J.L., Stern, L., Asmerom, Y., Edwards, R.L., Ito, E., 2004. Stable isotope variations in modern tropical speleothems: evaluating equilibrium vs. kinetic isotope effects. *Geochimica et Cosmochimica Acta* 68, 4381–4393.
- Mickler, P.J., Stern, L.A., Banner, J.L., 2006. Large kinetic isotope effects in modern speleothems. *Geological Society of America Bulletin* 118, 65–81.
- Müller, H., 1974. Pollenanalytischen Untersuchungen und Jahresschichtzählungen an der Eem-zeitlichen Kieselgur von Bisingen/Luhe. *Geologisches Jahrbuch*. A 21, 829–856.
- Müller, U.C., Kukla, G.J., 2004. North Atlantic Current and European environments during the declining stage of the Last Interglacial. *Geology* 32, 1009–1012.
- Müller, U.C., Sánchez Goñi, M., 2007. Vegetation dynamics in Southern Germany during Marine Isotope Stage 5 (~130 to 70 kyr ago). In: Sirocko, F., Claussen, M., Litt, T., Sánchez Goñi, M.F. (Eds.), *The Climate of Past Interglacials. Developments in Quaternary Science Series*, vol. 7. Elsevier, pp. 277–288.
- NGRIP Community Paper, 2004. High resolution record of Northern Hemisphere climate extending into the Last Interglacial period. *Nature* 431, 147–151.
- Oppo, D.W., McManus, J.F., Cullen, J.L., 2006. Evolution and demise of the Last Interglacial warmth in the subpolar North Atlantic. *Quaternary Science Reviews* 25, 3268–3277.
- Paillet, D., Bard, E., 2002. High frequency palaeoceanographic changes during the past 140,000 yr recorded by the organic matter in sediments of the Iberian margin. *Palaeogeography, Palaeoclimatology, Palaeoecology* 181, 431–452.
- Peer, H., Zimmer, W., 1980. Geologie der Nordrahmenzone der Hohen Tauern (Gasteiner Ache bis Saukarkopf-Großarlal). *Jahrb. Geol. Bundesanstalt*, Vienna 123, 411–466.
- Pflaumann, U., Sarnthein, M., Chapman, M., d'Abreu, L., Funnell, B., Huels, M., Kiefer, T., Maslin, M., Schulz, H., Swallow, J., van Kreveland, S., Vautravers, M., Vogelsang, E., Weinelt, M., 2003. Glacial North Atlantic: sea-surface conditions reconstructed by GLAMAP 2000. *Paleoceanography* 18.
- Prokopenko, A.A., Karabanov, E.B., Williams, D.F., Khursevich, G.K., 2002. The stability and the abrupt ending of the Last Interglaciation in Southeastern Siberia. *Quaternary Research* 58, 56–59.
- Rasmussen, T.L., Thomsen, E., Kuijpers, A., Wastegard, S., 2003. Late warming and early cooling of the sea surface in the Nordic seas during MIS 5e (Eemian Interglacial). *Quaternary Science Reviews* 22, 809–821.
- Rozanski, K., Araguás-Araguás, L., Gonfiantini, R., 1992. Relation between long-term trends in oxygen-18 isotope composition of precipitation and climate. *Science* 258, 981–985.
- Ruddiman, W.F., McIntyre, A., 1979. Warmth of the Subpolar North Atlantic Ocean during Northern Hemisphere ice-sheet growth. *Science* 204, 173–175.
- Sánchez Goñi, M.F., Turon, J.-L., Eynaud, F., Shackleton, N.J., 1999. High resolution palynological record off the Iberian margin: direct land-sea correlation for the Last Interglacial complex. *Earth and Planetary Science Letters* 171, 123–137.
- Sánchez Goñi, M.F., Loutre, M., Crucifix, M., Peyron, O., Santos, L., Duprat, J., Malaize, B., Turon, J.-L., Peypouquet, J.P., 2005. Increasing vegetation and climate gradient in western Europe over the Last Glacial inception (122–110 ka): data-model comparison. *Earth and Planetary Science Letters* 231, 111–130.
- Scholz, D., Mangini, A., Felis, T., 2004. U-series dating of diagenetically altered fossil reef corals. *Earth and Planetary Science Letters* 218, 163–178.
- Schotterer, U., Fröhlich, K., Gäggeler, H.W., Sandjordj, S., Stichler, W., 1997. Isotope records from Mongolian and Alpine ice cores as climate indicators. *Climatic Change* 36, 519–530.

- Schürch, M., Kozel, R., Schotterer, U., Tripet, J.P., 2003. Observation of isotopes in the water cycle—the Swiss National Network (NISOT). *Environmental Geology* 45, 1–11.
- Severinghaus, J.P., Sowers, T., Brook, E.J., Alley, R.B., Bender, M.L., 1998. Timing of abrupt climate change at the end of the Younger Dryas interval from thermally fractionated gases in polar ice. *Nature* 391, 141–146.
- Shackleton, N.J., Chapman, M., Sánchez Goñi, M.F., Pailler, D., Lancelot, Y., 2002. The classic marine isotope substage 5e. *Quaternary Research* 58, 14–16.
- Shackleton, N.J., Sánchez Goñi, M.F., Pailler, D., Lancelot, Y., 2003. Marine isotope substage 5e and the Eemian Interglacial. *Global and Planetary Change* 36, 151–155.
- Siddall, M., Rohling, E.J., Almogi-Labin, A., Hemleben, C., Meischner, D., Schmelzer, I., Smeed, D.A., 2003. Sea-level fluctuations during the last glacial cycle. *Nature* 423, 853–858.
- Sirocko, F., Claussen, M., Litt, T., Sánchez Goñi, M.F., Berger, A., Boettger, T., Diehl, M., Desprat, S., Delmote, B., Degering, D., Frechen, M., Geyh, M.A., Gröger, M., Kageyama, M., Kaspar, F., Kühl, N., Kubatzki, C., Lohmann, G., Loutre, M.F., Müller, U., Rein, B., Rosendahl, W., Roucoux, K., Rousseau, D.-D., Seelos, K., Siddall, M., Scholz, D., Spötl, C., Urban, B., Vautrans, M., Velichko, A., Wenzel, A., Widmann, M., Wünnemann, N., 2007. Chronology and climate forcing of the last four interglacials. In: Sirocko, F., Claussen, M., Litt, T., SánchezGoñi, M.F. (Eds.), *The Climate of Past Interglacials. Developments in Quaternary Science Series*, vol. 7. Elsevier, pp. 597–614.
- Skinner, L.C., Shackleton, N.J., 2006. Deconstructing Terminations I and II: revisiting the glacioeustatic paradigm based on deep-water temperature estimates: critical Quaternary stratigraphy. *Quaternary Science Reviews* 25, 3312–3321.
- Spötl, C., Vennemann, T.W., 2003. Continuous-flow isotope ratio mass spectrometric analysis of carbonate minerals. *Rapid Communications in Mass Spectrometry* 17, 1004–1006.
- Spötl, C., Fairchild, I.J., Tooth, A.F., 2005. Speleothem deposition in a dynamically ventilated cave, Obir Caves (Austrian Alps). Evidence from modern cave air and drip water monitoring. *Geochimica et Cosmochimica Acta* 69, 2451–2468.
- Spötl, C., Mangini, A., Richards, D.A., 2006. Chronology and paleoenvironment of Marine Isotope Stage 3 from two high-elevation speleothems, Austrian Alps. *Quaternary Science Reviews* 25, 1127–1136.
- Spötl, C., Holzkämper, S., Mangini, A., 2007. The Last and the Penultimate Interglacial as recorded by speleothems from a climatically sensitive high-elevation cave site in the Alps. In: Sirocko, F., Claussen, M., Litt, T., SánchezGoñi, M.F. (Eds.), *The Climate of Past Interglacials. Developments in Quaternary Science Series*, vol. 7. Elsevier, pp. 471–491.
- Sprovieri, R., Di Stefano, E., Incarbona, A., Oppo, D.W., 2006. Suborbital climate variability during MIS 5 in the central Mediterranean basin: evidence from calcareous plankton record. *Quaternary Science Reviews* 25, 2332–2342.
- Steinhauser, F., 1982. Verteilung der Häufigkeiten der Windrichtungen und der Windstärken in Österreich zu verschiedenen Tages—und Jahreszeiten. *Arbeiten aus der ZAMG, Vienna*, p. 53.
- Stirling, C.H., Esat, T.M., Lambeck, K., McCulloch, M.T., 1998. Timing and duration of the Last Interglacial: evidence for a restricted interval of widespread coral reef growth. *Earth and Planetary Science Letters* 160, 745–762.
- Tooth, A.F., Fairchild, I.J., 2003. Soil and karst aquifer hydrological controls on the geochemical evolution of speleothem-forming drip waters, Crag Cave, southwest Ireland. *Journal of Hydrology* 273, 51–68.
- Tzedakis, P.C., 2003. Timing and duration of Last Interglacial conditions in Europe: a chronicle of a changing chronology. *Quaternary Science Reviews* 22, 763–768.
- van Husen, D., 1987. Die Ostalpen und ihr Vorland in der letzten Eiszeit (Würm). Map 1: 500,000, Vienna (Geol. Bundesanstalt, Vienna).
- Veit, H., 2002. Die Alpen—Geoökologie und Landschaftsentwicklung. Eugen Ulmer Verlag, Stuttgart, Germany, 352pp.
- Vettoretti, G., Peltier, W.R., 2003. Post-Eemian glacial inception. Part I: The impact of summer seasonal temperature bias. *Journal of Climate* 16, 889–911.
- Vimeux, F., Cuffey, K.M., Jouzel, J., 2002. New insights into Southern Hemisphere temperature changes from Vostok ice cores using deuterium excess correction. *Earth and Planetary Science Letters* 203, 829–843.
- Waelbroeck, C., Labeyrie, L., Michel, E., Duplessy, J.C., McManus, J.F., Lambeck, K., Balbon, E., Labracherie, M., 2002. Sea-level and deep water temperature changes derived from benthic foraminifera isotopic records. *Quaternary Science Reviews* 21, 295–305.
- Wang, X., Neubauer, F., 1998. Orogen parallel strike-slip faults bordering metamorphic core complexes: the Salzach-Enns fault zone in the Eastern Alps, Austria. *Journal of Structural Geology* 20, 799–818.
- Wiedner, E., Scholz, D., Mangini, A., Polag, D., Mühlinghaus, C., Segl, P., 2008. Investigation of the stable isotope fractionation in speleothems with laboratory experiments. *Quaternary International*, in press.
- Wurth, S., Niggemann, S., Richter, D.K., Mangini, A., 2004. The Younger Dryas and Holocene climate record of a stalagmite from Hölloch Cave (Bavarian Alps, Germany). *Journal of Quaternary Science* 19, 291–298.
- Yuan, D., Cheng, H., Edwards, R.L., Dykoski, C.A., Kelly, M.J., Zhang, M., Qing, J., Lin, Y., Wang, Y., Wu, J., Dorale, J.A., An, Z., Cai, Y., 2004. Timing, Duration, and Transitions of the Last Interglacial Asian Monsoon. *Science* 304, 575–578.
- ZAMG, 1985. Klimadaten von Österreich. *Arbeiten der ZAMG, Vienna*, p. 63.